18

A BATHYMETRIC SIDESCAN SONAR SYSTEM

BY

STUART ROY

SUBMITTED IN PARTIAL FULFILMENT OF
THE REQUIREMENTS FOR THE DEGREE OF
MASTER OF SCIENCE IN ENGINEERING

UNIVERSITY OF CAPE TOWN
DECEMBER 1986

The University of Cape Town has been given the right to reproduce this thesis in whole or in part. Copyright is held by the author.

The copyright of this thesis vests in the author. No quotation from it or information derived from it is to be published without full acknowledgement of the source. The thesis is to be used for private study or non-commercial research purposes only.

Published by the University of Cape Town (UCT) in terms of the non-exclusive license granted to UCT by the author.

University of Cape Town

ABSTRACT

The design and construction of a bathymetric sidescan sonar system capable of operation over a 39 degree vertical sector is described. Field tests conducted at a dam site indicate that the completed system does not function as required. This is due to errors in the sonar depth measurement which are caused by reverberation resulting from the multiple scattering of sound from the dam floor. Recommendations are made so that future systems will be less susceptible to this interference source.

University of Cape Town

ACKNOWLEDGEMENTS

I would like to thank my supervisor, Professor P.N. Denbigh, for his insight, assistance and encouragement.

I am also grateful to the Institute for Maritime Technology for the use of their indoor tank and fresh water reservoir facilities.

Financial support for this work was provided by the Council for Scientific and Industrial Research Foundation for Research Developement.

CONTENTS

CHAPTER 1

INTRODUCTION

It is essential that the crews of large tankers and bulk carriers be aware of any obstacle or topographic feature on the sea floor, posing a threat to the safety of their vessel. A clear need for accurate, detailed and frequently updated hydrographic surveys of shallow shipping channels therefore exists.

A traditional charting technique is to run a survey vessel over the area of interest in a number of parallel lines, typically separated by between 50 m and 150 m. An echo sounder is used to determine the depth of the sea bottom directly beneath the ship.

A major shortcoming of this technique is that the sea floor between sounding lines remains uncharted. A conventional sidescan sonar may be used to obtain a qualitative picture of the uncharted sea floor area. Hopefully, this indicates topographical feature and obstacles which pose a threat to shipping and require further investigation with the echo sounder. Such feature will not always be apparent from conventional sidescan sonar records and consequently the completed chart may contain considerable inaccuracies.

By combining the rapid area coverage of a sidescan sonar with the depth measuring capability of an echo sounder, a bathymetric sidescan sonar system developed by Denbigh (Denbigh, 1979) overcomes the shortcomings of the survey technique described above. The system operates in a similar fashion to a conventional sidescan sonar, with the exception that in addition to providing an indication of backscattered

amplitude, it simultaneously provides a continuous indication of sea bed depth. Since each depth measurement is made in a small elemental sea bed area, corresponding to the resolution cell of a conventional sonar, the system is capable of high resolution operation.

Denbigh has described the design of a bathymetric sidescan sonar system capable of operation over a 19 degree vertical sector (Denbigh, 1983). It is desirable that the vertical coverage of the system be extended.

In this thesis, the design and construction of a bathymetric sidescan sonar capable of operation over an increased vertical sector of 39 degrees is described. Field tests of the completed system, conducted in a large water tank and at a dam site, indicate that it does not operate as required.

Reverberation caused by multiple scattering between feature on the dam floor is identified as an interference source, suggesting a fundamental problem with the bathymetric sidescan sonar. A theoretical investigation is undertaken and indicates that the sonar system receivers are particularly susceptible to interference caused by multiple scattering between feature on the dam floor. Based on the theoretical investigation, recomendations are made enabling future systems to be less susceptible to this interference source.

CHAPTER 2

SYSTEM OVERVIEW

In this chapter the principle of operation and electronic implementation of the bathymetric sidescan sonar is described.

2.1 Principle of depth measurement.

To measure sea bed depth out sideways to the direction of travel of a ship or towed body, it is necessary to determine the slant range and declination angle of the elemental sea bed areas insonified by the sonar system. Fig. 2.1 depicts the manner in which the vertical fan beam of a conventional sidescan sonar insonifies a narrow swath of sea floor.

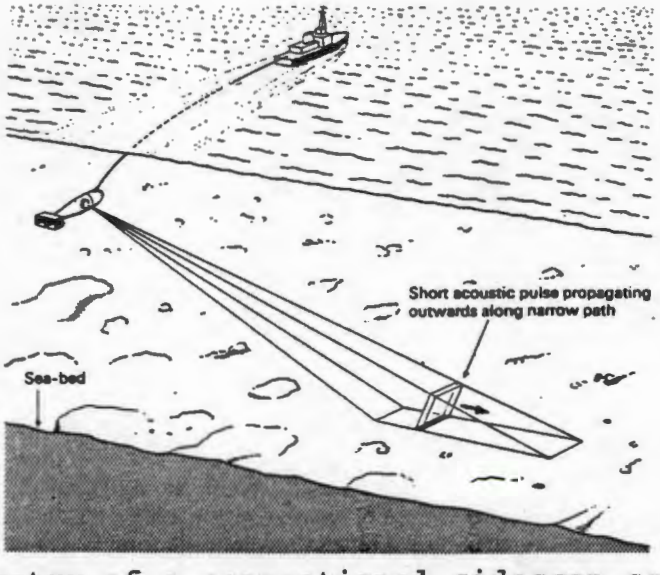

Fig. 2.1 Geometry of a conventional sidescan sonar system. (From Denbigh, 1983)

The depth d_i of an elemental seabed area A_i insonified by the acoustic transmit pulse may be calculated if its slant range r_i and declination angle θ_i are known. The slant range is determined by precisely measuring the two way propagation time t_i, of the echo return. The depth d_i is simply

$$d_i = \frac{ct_i}{2} \sin \theta_i$$

while the horizontal range x_i is

$$x_i = \frac{ct_i}{2} \cos \theta_i$$

where c is the velocity of sound propagation in water.

2.2 Phase difference technique.

If the acoustic transmit pulse produced by a sidescan sonar is of a short duration, the wavefronts backscattered from the sea bed are circular and centred about the elemental areas from which they originate. Fig. 2.2 shows echo wavefronts backscattered from various points along the sea floor and indicates that the inclination of these wavefronts to the vertical equals the declination angle from which they originate. A detailed study of this assumption has been made by Denbigh (Denbigh, 1980).

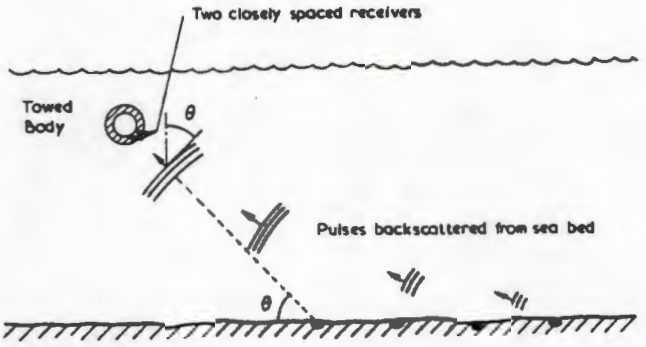

Fig. 2.2 Echo wavefronts returning from various points along an insonified swath.
(From Denbigh, 1983)

The bathymetric sidescan sonar determines the declination angle of the incoming acoustic wavefronts by precisely measuring the difference in arrival time of a wavefront at two closely spaced receivers. The principle behind the determination of declination angle may be understood by examining Fig. 2.3 which shows the two receivers separated by a distance d and inclined at an angle α to the vertical. Incoming acoustic wavefronts are shown incident at an angle β to the receivers. The scaling of the diagram has been exaggerated for clarity.

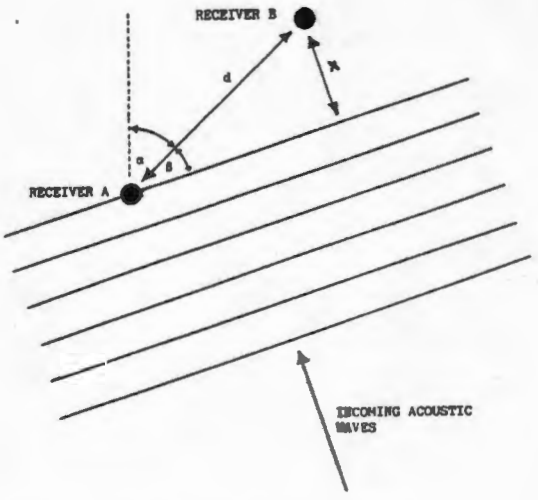

Fig. 2.3 Receiver geometry.

The wavefronts incident on the receivers are approximately linear, as long as the receiver separation d is small. On reaching A, the wavefronts must travel a distance x further before reception by B. The additional path length x introduces a phase shift ϕ between the signals appearing at the receiver outputs.

$$\phi = \frac{2\pi x}{\lambda} \tag{2.1}$$

by simple geometry

$$\sin \beta = \frac{x}{d} \tag{2.2}$$

Combining 2.1 and 2.2

$$\phi = \frac{2\pi d}{\lambda} \sin \beta$$

The declination angle of the incoming wavefronts is therefore

$$\theta = \alpha + \sin^{-1} (\lambda\phi/2\pi d) \tag{2.3}$$

Since phase may only be unambiguously resolved over 360 electrical degrees, a limit is imposed on the vertical sector over which the elevation angle of incoming wavefronts may be uniquely determined. The ambiguity points $\pm\theta_a$, which indicate the limits of this sector, are symmetrically placed about the receiver boresights and occur at elevation angles at which incoming wavefronts produce ±180 degrees of phase shift between the receiver outputs. The theoretical ambiguity points are

$$\theta_a = \pm \sin^{-1} (\lambda/2d) \tag{2.4}$$

A receiver separation of one wavelength, results in a system capable of unambiguously resolving elevation angle over a ±30 degree sector. A small receiver separation is required if a large unambiguous sector is to be realized.

2.3 Implementation.

A block diagram of the bathymetric sidescan sonar system, indicating the partitioning of the experimental system into hardware and software sections, is shown in Fig. 2.4.

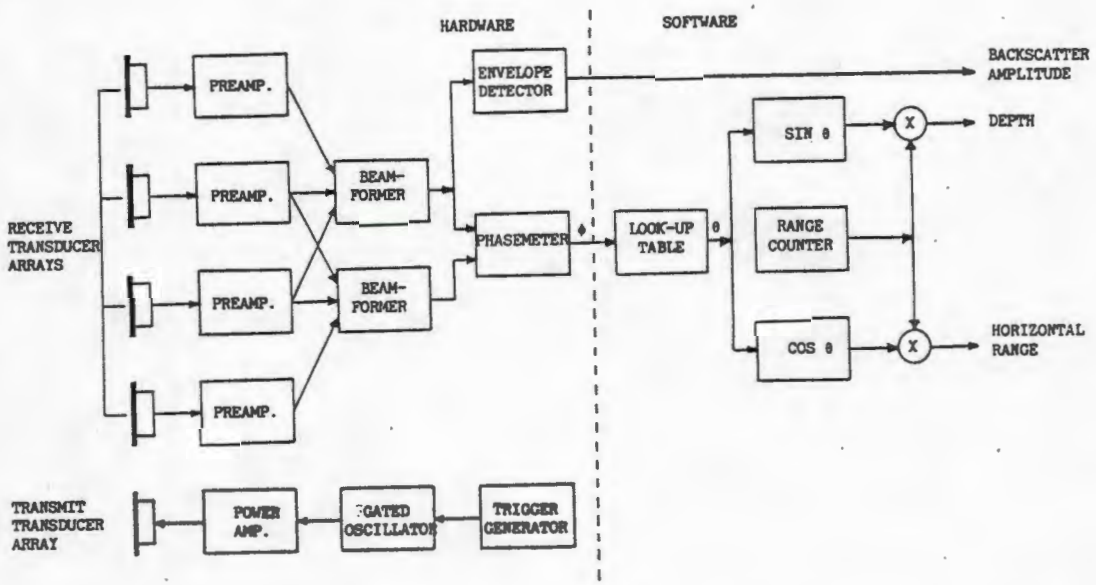

Fig. 2.4 Schematic block diagram of the bathymetric sidescan sonar system.

The electronic circuitry required to implement the system is relatively straightforward and only a brief description of the more important aspects follows. Relevant circuit diagrams are provided in appendix A.

Receive preamplifiers.

For reasons which become apparent in chapter 3, the receivers are formed from interleaved transducer arrays. Prior to forming the receive beams, the transducer outputs are each amplified by a low noise tuned preamplifier. The preamplifiers are matched to their respective transducers by carefully choosing the primary inductance of the amplifier input transformers so that the clamp capacitances of the transducers are tuned out at resonance (Runciman, 1986).

The transducer matching and circle diagrams are shown in appendix B.

To ensure that the phase of the signals appearing at the transducer outputs remain undisturbed by the preamplifier circuitry, the frequency responses of the preamplifiers are carefully matched. Since the resonant frequencies and bandwidths of the transducers are not identical, the preamplifier bandwidths are made sufficiently narrow so as to dominate those of the transducers and hence determine the overall frequency response of the receivers.

Phasemeter.

The amplitude of the backscattered sound encountered by a sidescan sonar system fluctuates rapidly over a considerable amplitude range. As the accuracy of the bathymetric sidescan sonar depth measurement is dependent on the precision with which the phasemeter indicates the receiver phase difference, the phasemeter must be capable of accurate operation over a large dynamic range.

The receiver phase measurement is made independent of reverberation level by hard limiting the receiver outputs and using these to produce a pulse train whose duty cycle represents the receiver phase difference. A phase inversion is introduced into one of the input channels enabling the phasemeter to provide an indication of phase over a ±180 degree range. An analog representation of the phase measurement is obtained by extracting the dc component of the variable duty cycle pulse train by low pass filtering. A block diagram of the phasemeter which includes timing waveforms, is shown in Fig. 2.5.

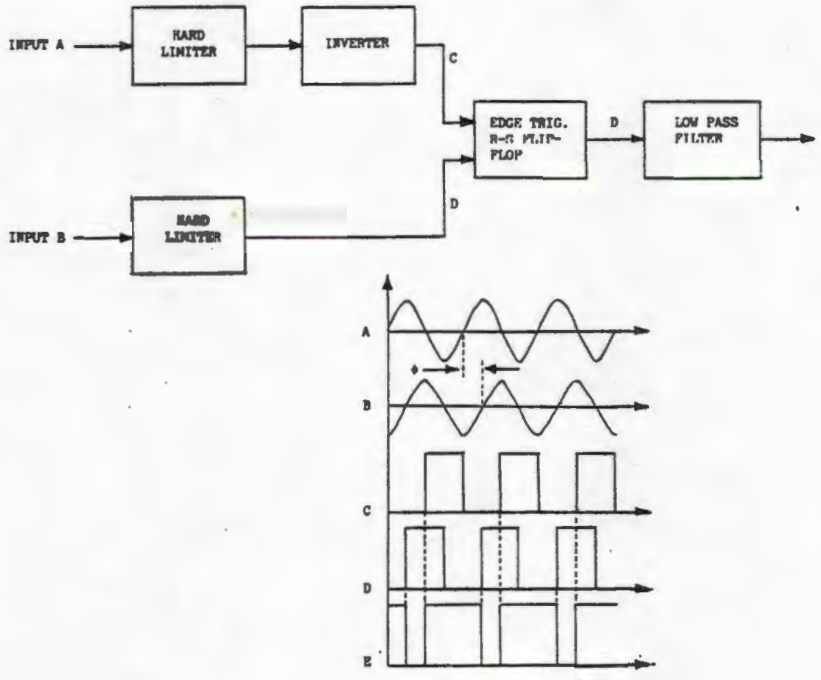

Fig. 2.5 Schematic block diagram of phasemeter.

Transmitter gating.

Due to the sensitivity of the phase difference technique to interference, transmitter breakthrough caused by imperfect gating of the transmit oscillator must be eliminated. This is achieved by continuously running the transmit oscillator at 712 kHz, twice the sonar operating frequency. A 316 kHz transmit pulse is generated by activating a gate and frequency divider circuit which halves the oscillator frequency while the gate is open. As any transmitter breakthrough occurs at twice the operating frequency, the narrow bandwidths of the transducer arrays ensure that negligible acoustic interference occurs during the sonar listen period.

Data capture and storage

To simplify implementation of the experimental sonar system and increase its flexibility, the processing of the phase waveform to yield depth information was not performed in real time. Instead, a Phillips PM 3055 30 Mhz digital storage oscilloscope equipped with a IEEE-488 bus, was used to capture envelope and phase waveforms. An HP 85 microcomputer was interfaced to the oscilloscope via a HPIB port. A modular control program listed in appendix B facilitated computer control of the oscilloscope and the downloading and storage of captured data on flexible disc for future processing.

CHAPTER 3

TRANSDUCER ARRAYS

If the receivers are to operate over a large unambiguous sector, they must be constructed from narrow closely spaced transducers. Due to the small transducer dimensions, the closely spaced receivers are particularly susceptible to mutual coupling. This disturbs the receiver phase measurement, causing the receiver phase difference response to become non monotonic. Consequently, it may no longer be possible to unambiguously determine the elevation angle of incoming acoustic waves.

In this chapter, a construction technique is presented, enabling the requisite receiver separation to be attained while ensuring that the receiver phase difference response remains a single valued function of elevation angle. The completed receivers are capable only of determining the elevation angle of sound originating from a single direction at any instant in time. Before the receivers can be used to determine the declination angle of sound backscattered from the sea floor, it is therefore necessary to eliminate multipath interference caused by reflection at the sea surface. This is achieved by using a side baffle to shadow the receive arrays from the sea surface. Finally, the design of a directive transmit transducer array is described.

3.1 Beam formation.

To ensure that the receiver phase measurement corresponds to the direct path reverberation only, a side baffle is used to eliminate multipath interference caused by reflection at the sea surface. To minimize the effect the introduction of the baffle has on the backscatter sound field, it is necessary to reduce the sensitivity of the receivers in the direction of the baffle edge (refer to section 3.5).

The requirement that the receive beams be narrow, suggests the use of wide transducer arrays which are directive in the vertical plane. To avoid a reduction in unambiguous sector caused by a consequent increase in the separation of the receiver phase centres, the receive beams are formed from interleaved transducer arrays.

Line arrays with appropriate connections are used to form two interleaved receivers (Denbigh, 1983). One receiver is comprised of the top three elements to which a triangular amplitude shading of 1/2, 1, 1/2 is applied, while the second receiver consists of the lower three elements to which the same amplitude weightings are applied. This configuration results in the separation between the receiver phase centres being less than the physical receiver dimensions. The interleaved receivers, together with their triangular weightings are shown in Fig. 3.1.

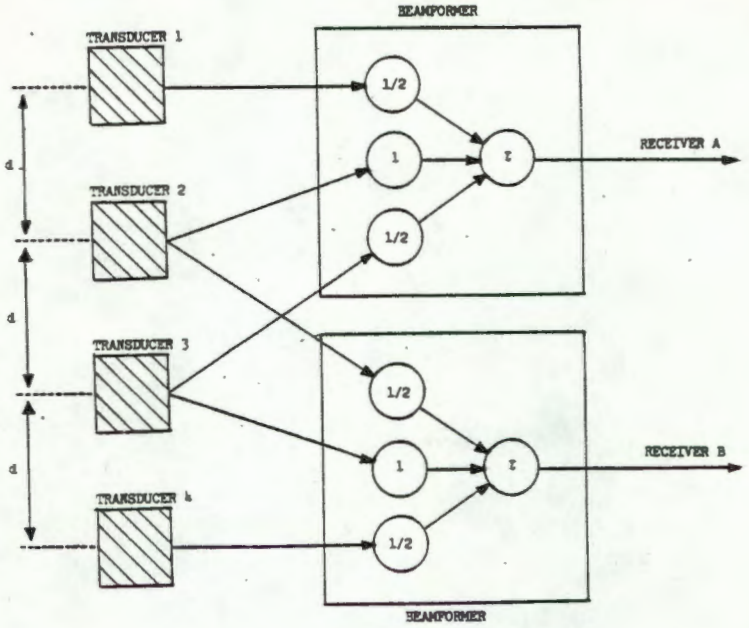

Fig. 3.1 Formation of receive beams using interleaved transducer arrays.

3.2 Mutual coupling.

If the phase difference technique is to unambiguously determine the declination angle of backscattered reverberation, the phase measurement made by the receivers should be identical to that existing in the free backscatter sound field.

The occurrence of mutual coupling between receivers results in their outputs not being entirely due to incident acoustic waves alone. Consequently, the phase of the signals appearing at the receiver outputs is disturbed and no longer identical to that existing in the free sound field. Fig. 3.2 shows a vector representation of the outputs R_A, R_B of two receivers due to incident acoustic waves and includes the effects of mutual coupling components S_{BA} and S_{AB}. Since the phase of the coupling components are unknown, the locii of the receiver outputs are shown.

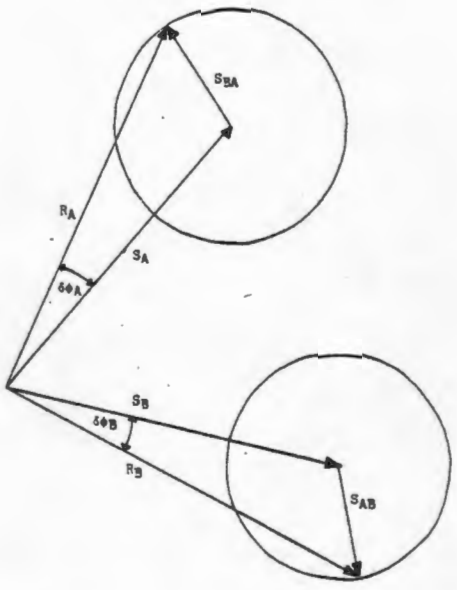

Fig. 3.2 Vector representation of receiver phase errors caused by mutual coupling.

The maximum error in the receiver phase difference measurement occurs when S_{BA} leads S_A by 90 degrees while S_{AB} lags S_B by 90 degrees. The resulting phase error $\delta\phi_{max}$ is

$$\delta\phi_{max} = \tan^{-1}(S_{BA}/S_A) + \tan^{-1}(S_{AB}/S_B)$$

If the mutual coupling components are 20 dB below the level of the incident sound, a worst case phase error of 11.4 degrees occurs. Mutual coupling manifests itself as asymmetries in the amplitude and phase difference responses of the receivers. Sufficient decoupling must therefore be provided between receivers to ensure that the receiver phase difference response remains a single valued function of elevation angle.

In order that the receivers be capable of determining the declination angle of incoming wavefronts over a ±26 degree sector, a receiver separation of 1.1 wavelengths is needed. The requirement of a small receiver separation necessitates the use of narrow transducer elements. A major problem with small ceramic transducers, in the region of 1 wavelength in width, is that they do not vibrate simply as pistons (Smith et al, 1979). Due to the small aspect ratio of width

to thickness dimension, a significant amount of energy is coupled into the transverse vibratory mode. This causes the whole transducer shape to distort and there is thus a significant displacement of the transducer sidewalls. The use of small dimension ceramic transducers causes the receivers to be particularly susceptible to mutual coupling. Work done by Denbigh (Denbigh, 1983), indicates that an airgap is required between transducers if the requisite receiver separation and decoupling is to be attained.

3.3 Air-spaced arrays.

An air-spaced array may be realized by mounting transducers directly on a rigid front face material. A particularly attractive feature of this technique is that the transducers are airbacked, thus avoiding a potential source of interference arising from internal reflections of incident acoustic waves within an imperfect backing material. If the front face material is chosen so that its acoustic properties are similar to that of water, it will act as an acoustic window and the losses introduced by it will be small. By carefully choosing the thickness of the front face material, the acoustic window acts as an impedance transformer, thereby increasing the efficiency of sound energy transfer between water and transducers.

Hood has developed a simple technique for the construction of compact multi-element 300 kHz transducer arrays. Polycarbonate is used as an acoustic window material. Transducers are bonded directly to the Polycarbonate while coupling paths are minimized by machining slots between adjacent transducers. Hood investigated a number of Polycarbonate configurations and determined that a 6 mm thick front face with 2 mm decoupling slots provided maximum efficiency and decoupling. This construction technique is illustrated in Fig. 3.3. The intensity reflection coefficients occurring at each interface are also indicated.

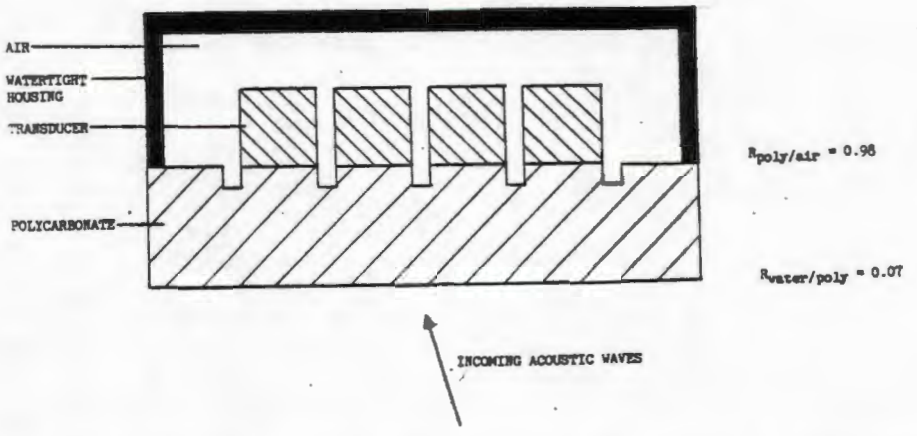

Fig. 3.3 Transducer array construction using a Polycarbonate acoustic window.

It is evident that the Polycarbonate air interface is almost a perfect pressure release surface. A small impedance discontinuity exists however at the water Polycarbonate interface. Fortunately, experiments involving the masking off of areas of the Polycarbonate front face with a closed cell foam material, indicated that the discontinuity was too small to cause interference by allowing incident sound to become trapped within the Polycarbonate and strike transducers after multiple reflections within the acoustic window.

An investigation of the effect of Polycarbonate thickness on receiver performance indicated that the transducer directivity and phase difference responses were not substantially affected by a reduction in Polycarbonate thickness. Attempts at constructing the receive arrays at a frequency of 185 kHz by frequency scaling the dimensions of Hood's suggested configuration were unsuccessful however. The resulting receiver directivity patterns were irregular and the phase difference response was non monotonic. The disappointing receiver performance is believed due to mutual coupling.

3.4 Transmission line model.

The decoupling requirements of the closely spaced receivers are far more stringent than those imposed by the applications for which the configuration suggested by Hood is intended. A simple transmission line model is applied to the Polycarbonate acoustic window to enable the optimum thickness, slot depth and position to be determined.

If the Polycarbonate transducer configuration is considered a receiver, then the transmission line model shown in Fig. 3.4 may be applied.

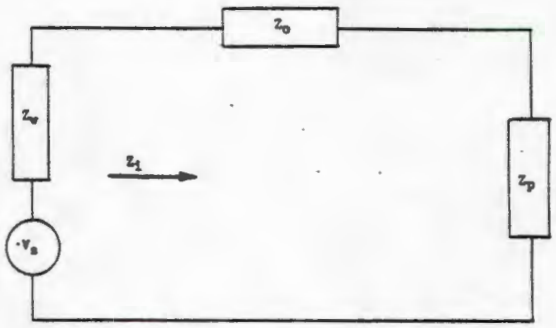

Fig. 3.4 Transmission line model.

The arrival of acoustic waves at the Polycarbonate front face is modelled by a voltage source whose impedance Z_w is equivalent to the acoustic impedance of water. The Polycarbonate acoustic window is depicted by the transmission line of characteristic impedance Z_o, equal to the acoustic impedance of the Polycarbonate, while the Piezoelectric transducers are modelled by a lumped impedance Z_p, equivalent to the acoustic impedance of the transducer elements.

To ensure the efficient transfer of acoustic energy from the water to the Piezoelectric transducers, an impedance transformer is required to transform the relatively low acoustic impedance of the water to the high impedance of the Piezoelectric transducers.

If the Polycarbonate acoustic window is an odd multiple of quarter wavelengths thick, the impedance Z_i seen looking into the acoustic window is

$$Z_i = \frac{Z_o^2}{Z_p}$$

By making the Polycarbonate acoustic window an odd multiple of quarter wavelengths thick, a reasonable receiver efficiency is achieved. Assuming a velocity of sound propagation in Polycarbonate of 2220 m/s (Hung and Goldstein, 1983) and a sound frequency of 316 kHz, a quarter wavelength Polycarbonate acoustic window is 1.8 mm thick. It was determined that Polycarbonate of this thickness is not sufficiently rigid to be used as an acoustic window. In any event, the Polycarbonate configuration suggested by the 1/4 wavelength thick transmission line model is unsuitable for use in implementing the receivers.

A 3/4 wavelength thick Polycarbonate front face is suitable for use as an acoustic window. The Polycarbonate configuration suggested by the 3/4 wavelength transmission line model and adopted in the construction of the receivers is shown in Fig. 3.5.

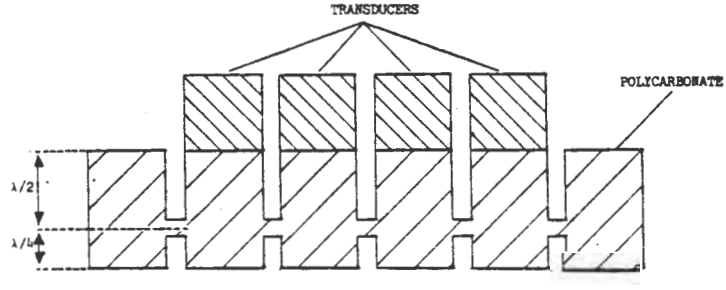

Fig. 3.5 3/4 wavelength Polycarbonate configuration.

Pressure maxima and velocity minima occur at both the high impedance transducer face and at a point a quarter wavelength from the low impedance water face. It is believed that the effects of boundary discontinuities on the incoming acoustic waves may be reduced by positioning the slot bottoms close to a velocity minimum. Decoupling between transducers is

therefore provided by 1/2 wavelength deep 0.6 mm wide slots machined into the air face of the Polycarbonate acoustic window. If additional decoupling is required, 1/4 wavelength deep slots may be machined into the Polycarbonate water face. If these slots are to provide the necessary decoupling however, they must be filled with a material capable of maintaining a large impedance discontinuity in the presence of water. This complicates the construction of the receivers and for this reason the slots were left unfilled.

To minimize spatial distortion of the incoming acoustic waves over the receive aperture, the discontinuities occurring at the outermost transducers are removed by placing a dummy transducer alongside each. The acoustic window was constructed from 6 mm thick Polycarbonate, the closest commercially available thickness to the required 3/4 wavelength (5.3 mm) dimension. Due to the accuracy with which the slots were machined, a Polycarbonate thickness of approximately 0.5 mm is required to remain between the air and water decoupling slots. The slot boundaries were therefore placed 0.25 mm above and below the velocity minimum occurring a quarter wavelength or 1.8 mm from the water face. A photograph of the front face of the completed receivers in which the slot positions are clearly visible is shown in Fig. 3.6.

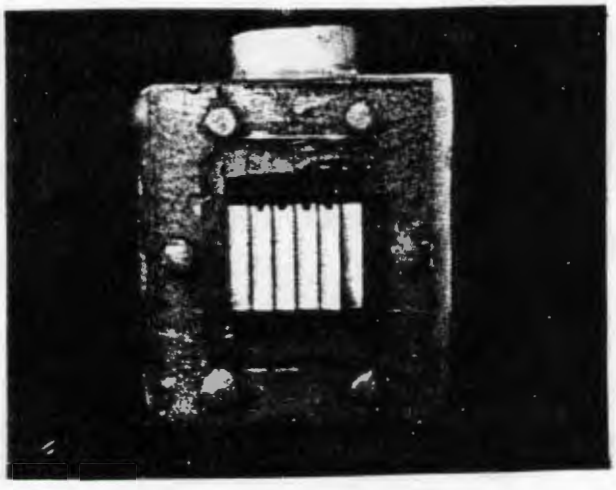

Fig. 3.6 Completed receive arrays.

3.4.1 Results.

The directivity patterns and phase difference response of the two receive beams are shown in Fig. 3.7. To facilitate comparison of these results, a reference receive array was formed from transducers mounted on a 6 mm thick Polycarbonate acoustic window. No decoupling slots were provided. The resulting receiver directivity patterns and phase difference response are presented in Fig. 3.8.

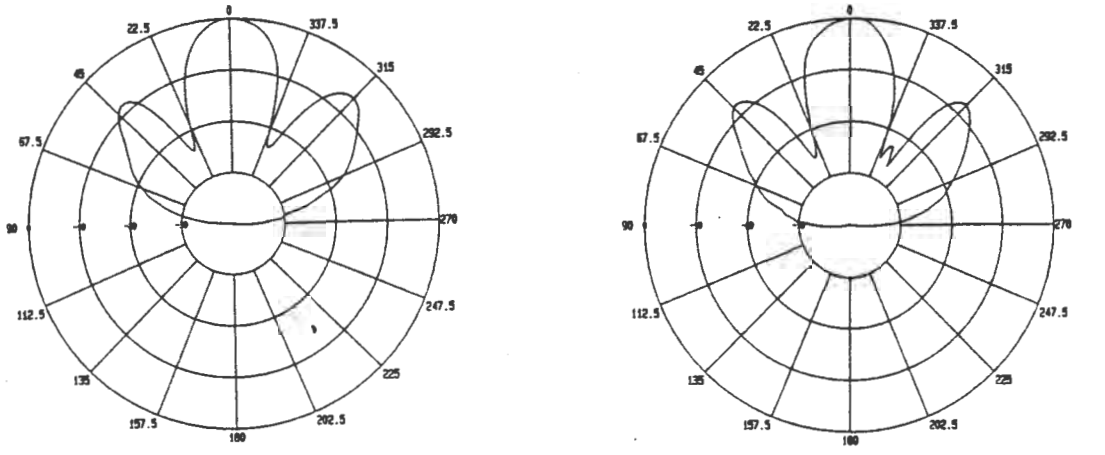

(a)

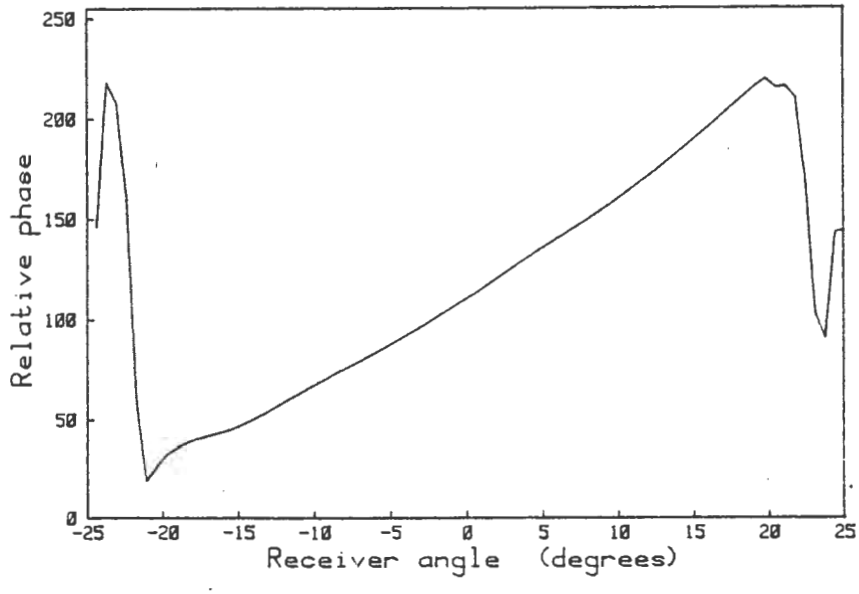

(b)

Fig. 3.7 Receiver (a) directivity plots
(b) phase difference response.

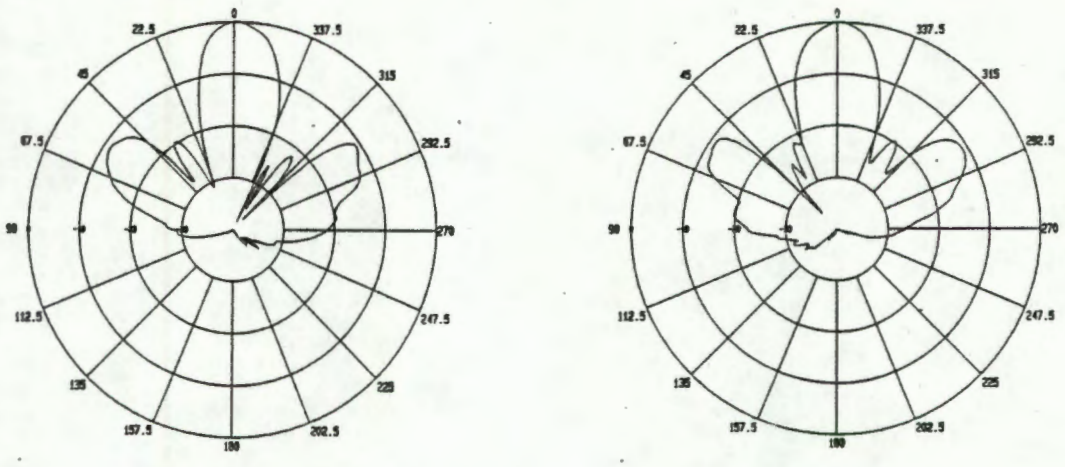

(a)

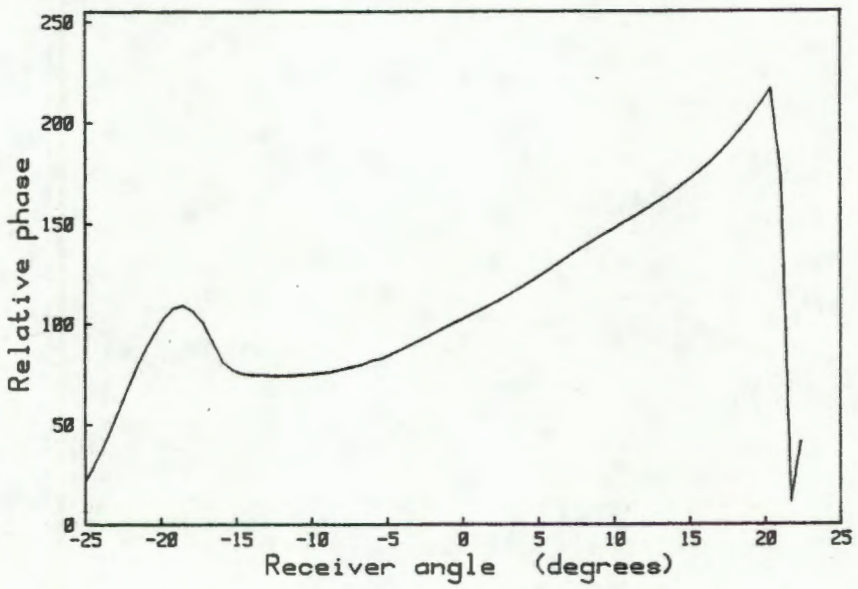

(b)

Fig. 3.8 Reference array (a) directivity plots
(b) phase difference response.

The main beams of both receiver configurations are well matched and show no signs of any irregularity caused by mutual coupling. The notches in the directivity patterns of the receivers shown in Fig. 3.7 are approximately 23 dB deep and occur at ±25 degrees. This is in excellent agreement with the ±26 degree separation expected from the 4.8 mm wide ceramics and 0.6 mm slot width.

The nulls of the directivity patterns shown in Fig. 3.8 are generally deeper than 23 dB. The phase difference response of this array deviates considerably from the ideal at an angular displacement corresponding to a null in the directivity response of the receivers. Deviations from ideal behaviour are expected to manifest themselves in the region of a receive null as small errors in the amplitude weighting of individual transducers, caused by mutual coupling, produce large phase perturbations in the receiver outputs. Strictly speaking, the elevation angle of incoming wavefronts may only be unambiguously determined over a 19.5 degree sector by this array.

The useful unambiguous sector of the phase difference response shown in Fig. 3.7 is ±21 degrees, an increase of 24.5 degrees over that of the reference array. The unambiguous sector is ±4 degrees smaller than predicted by the transducer separation. Beyond the ±21 degree sector, the phase difference response is no longer single valued. This is due to the critical nature of the vector addition performed by the beamformers at angles close to the receive nulls. It is believed that the useful unambiguous sector may be extended to include the entire ±25 degree sector by further increasing the decoupling betweeen transducers. This may be achieved by inserting a suitable material into the slots on the Polycarbonate water face. For completeness, the directivity patterns of the individual transducer elements for the two configurations are shown in appendix D.

3.5 Receiver side baffle.

The phase difference technique described in chapter 2 is capable only of determining the elevation angle of acoustic wavefronts originating from a single elevation angle at any instant in time. If acoustic waves from more than a single direction are simultaneously incident on the receivers, errors are introduced into the receiver phase measurement and the phase difference technique breaks down.

Before the receivers may be used to determine the declination angle of sound backscattered from the sea floor, it is therefore necessary to ensure that the phase measurement performed by the receivers corresponds to the direct path signal only. As the sea surface is almost a perfect reflector of sound, it is imperative that any multipath interference caused by reflection at the sea surface be eliminated. This is achieved by using side baffles to shadow both the transmit and receive transducer arrays from the sea surface.

Due to the critical nature of the phase measurement performed at the receivers, it is important to minimize the effects the introduction of a side baffle might have on the backscatter sound field. Particular care must be taken in positioning the baffle edge to avoid interference between the incoming acoustic waves and a wave diffracted from the baffle edge. Edge diffraction effects may be reduced by increasing the separation between the receivers and the baffle edge. This approach leads however to a baffle whose dimensions make it unwieldly. An alternative approach suggested by Denbigh (Denbigh, 1983) is to reduce the sensitivity of the receivers in the direction of the baffle edge. The triangular weighting scheme described in section 3.1, introduces a null into the vertical directivity response of the receivers. The elevation angles at which the receive nulls occur coincide with the receiver ambiguity points. The baffle edge may therefore be placed in a receiver null without reducing the unambiguous sector over which the sonar operates.

A reflective side baffle is used to shadow the receive arrays from the sea surface. The baffle is constructed from Aluminium to which a closed cell foam material is bonded. The baffle dimensions are such that its edge is positioned in the receiver nulls. The geometry of the receiver system with side baffle is shown in Fig. 3.9 while the directivity patterns and phase difference response of the receivers with the side baffle present, are shown in Fig. 3.10.

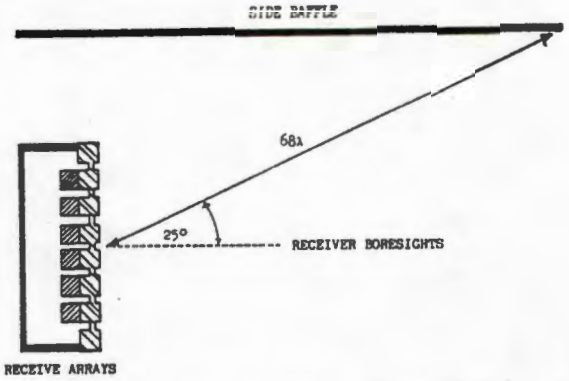

Fig. 3.9 Receiver side baffle geometry.

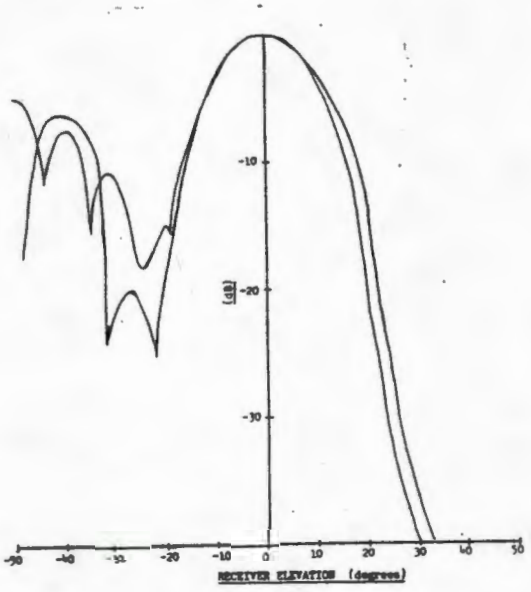

(a)

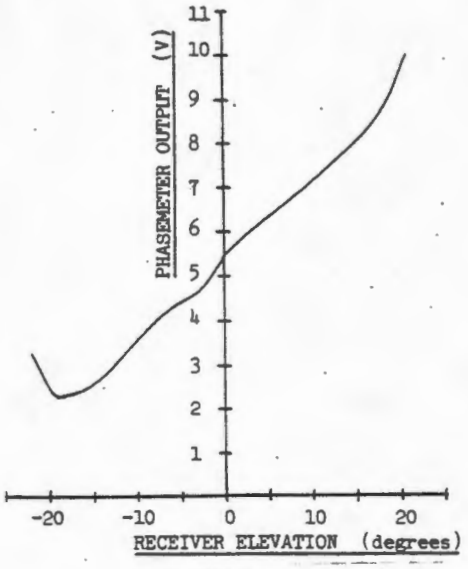

(b)

Fig. 3.10 Receiver side baffle combination
(a) directivity responses
(b) phase difference response.

The receive beams are well matched and exhibit no irregularities caused by edge diffraction throughout their main beams. It is evident that the receiver sensitivities are extremely low in the shadow region beyond +25 degrees. Large receiver sidelobes are apparent at angles smaller than -25 degrees. These are caused by reflections off the underside of the baffle and are unimportant as they occur outside the unambiguous sector of the receivers. The receiver directivity responses begin to deviate from the ideal at angles slightly larger than the -25 degree null angles. This is caused by reception, arising from the finite depth of the receive nulls, of acoustic waves reflected from the baffle edge. The phase of the direct path signals are disturbed and the angular sector over which arrival angle may be determined by the receiver baffle combination is +21 to -18 degrees, a decrease of 3 degrees over that produced without the baffle.

3.6 Transmit array.

The receivers are constructed from 5.3 wavelength long transducers, which result in an 11 degree wide main beam. The horizontal directivity is of the classical sin x/x shape and contains appreciable sidelobe levels. The resolution of the bathymetric sidescan sonar is therefore determined by the beamwidth of the transmit array. A line array formed from twelve 5.34 wavelength long Piezoelectric transducers is used as a transmitter. This results in a theoretical horizontal beamwidth of 0.9 degrees.

The directivity of a line array consisting of N transducers of length l and separation d is of the form

$$D(k\sin\theta) = \frac{\sin\left(\frac{kl\sin\theta}{2}\right)}{\frac{kl\sin\theta}{2}} \quad \frac{\sin\left(\frac{Nkd\sin\theta}{2}\right)}{\sin\left(\frac{kd\sin\theta}{2}\right)}$$

where k is the wavenumber $\frac{2\pi}{\lambda}$

Grating sidelobes occur when

$$\frac{kd}{2}\sin\theta = n\pi \qquad n = 1,2,3,\ldots$$

If l=d, the grating sidelobes disappear. Due to the large receiver beamwidth, it is desirable that the sidelobe levels of the transmit array be small. This is achieved by ensuring that the line array is formed from closely spaced transducers. The maximum transducer separation occurring in the transmit array is 5.34 wavelengths. Consequently, the maximum theoretical grating sidelobe level is 34 dB below the main beam. The transmit array was constructed by mounting transducers on a rigid closed cell foam material and encapsulating them in epoxy after suitable electrical connections had been made to their conductive faces. The completed array is shown in Fig. 3.11.

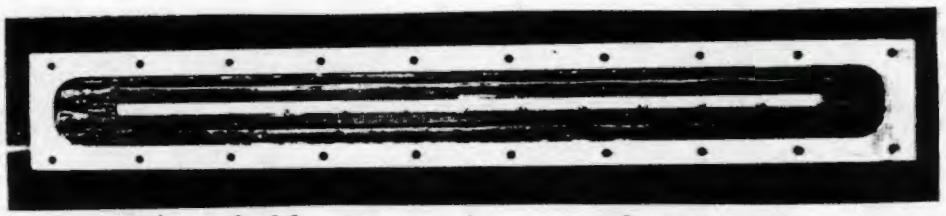

Fig. 3.11 Transmit transducer array.

The transmit array is constructed from 1 wavelength wide transducers. These produce a theoretical vertical beamwidth of 56 degrees. The vertical directivity pattern of the transmit array is shown in appendix D. A side baffle is used to prevent the radiation of acoustic energy by the transmit array in the direction of the sea surface. Unlike the receivers, the positioning of the transmitter side baffle is not critical. The sea surface is shadowed by a flat reflective baffle, positioned parallel to the array boresight. The baffle dimensions are such that its edge is a distance 9 wavelengths from the transducers. A photograph of the transmitter side baffle is included in section 4.2.

CHAPTER 4

TESTING

In this chapter, tests conducted in a large water tank and at a dam site are described. These indicate that discontinuities present in the receiver phase difference measurement are caused by multipath interference. An experiment using a sidescan sonar with separated transducer arrays is described and indicates that reverberation arising from multiple scattering between feature on the dam floor is of sufficient magnitude to severely limit the performance of the bathymetric sidescan sonar system.

Finally, the mapping of a sector of the dam floor is described and a 3-dimensional perspective picture of the bottom presented. Due to the unwanted effect mentioned above, it was necessary to smooth out spikes in the receiver phase difference measurement by spatially averaging the raw phase data. Consequently, the plot has a disappointing range resolution, much less than that corresponding to the transmit pulse length.

4.1 Tank tests.

Initial testing of the bathymetric sidescan sonar system involving the observation and recording of envelope and phase waveforms produced by backscatter from a known surface, were conducted at the indoor tank facility of the Institute for Maritime Technology, Simonstown. The water tank dimensions are 20 m x 10 m x 10 m. The transducers were mounted at a depth of 1 m and a tilt angle of 55 degrees. The position of the transducer arrays within the water tank are shown in Fig. 4.1.

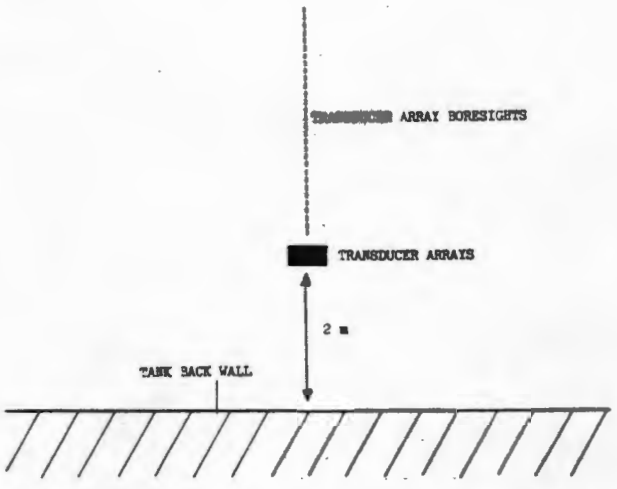

Fig. 4.1 Transducer array geometry during tank tests.

During the tank and other tests described in this chapter, a transmit pulse width of 50 μs was used. The transmitter pulse repetition rate was kept sufficiently low to ensure that reverberation from successive transmit pulses did not overlap, causing interference.

The bathymetric sidescan sonar system did not operate as required. A number of spikes which clearly did not correspond to feature on the tank bottom were apparent throughout the phase ramps occurring during the backscatter returns. These coincided with nulls in the echo signal. The phase spikes cause depth errors during subsequent processing of the phase data and while these may be reduced by spatial averaging, this leads to a sharp decrease in the range resolution of the sonar system. It is important therefore that the cause of the phase spikes be determined.

The envelope detector and phasemeter output waveforms for a typical backscatter return are shown in Fig. 4.2. Each waveform is digitized at 25 μs intervals over a slant range extending from 9.8 m to 20.3 m. Sound backscattered from the tank bottom within the unambiguous sector of the receivers is first received 16 ms after the transmit bang. The phasemeter output ramps upwards thereafter as the declination angle from which the backscattered reverberation originates decreases as the transmit pulse propagates outwards.

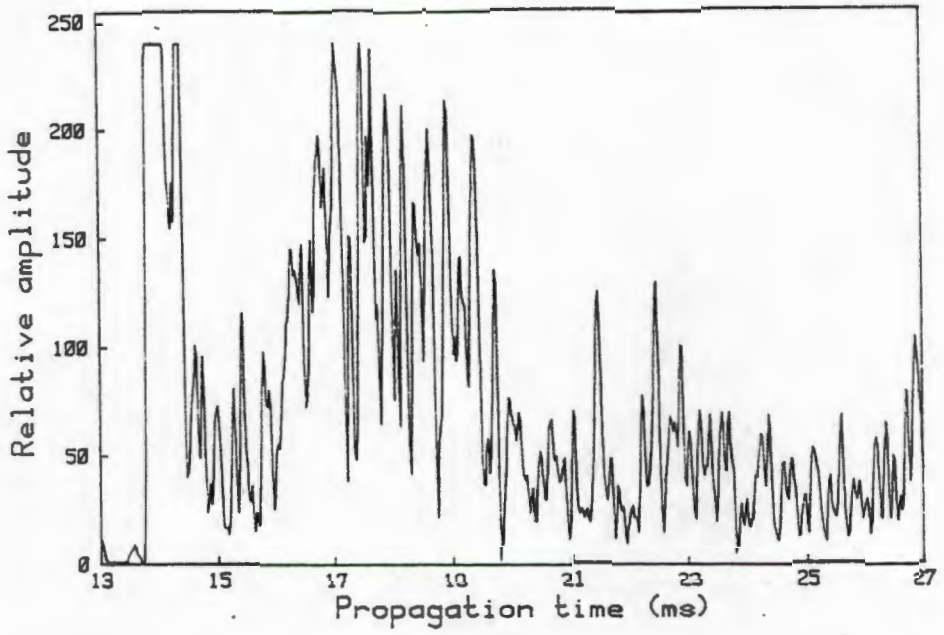

(a)

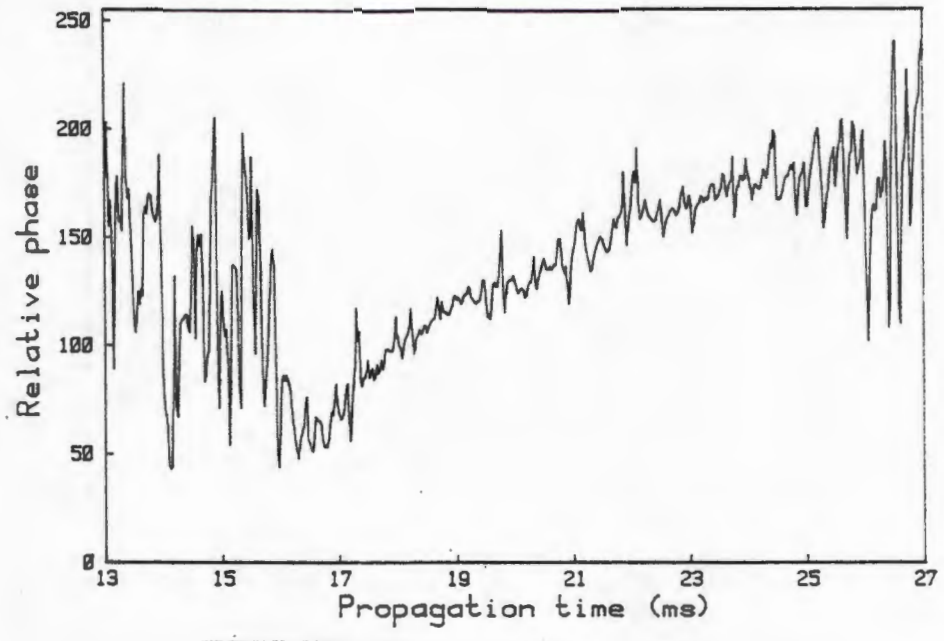

(b)

Fig. 4.2 Typical sonar waveforms recorded during tank tests
(a) envelope detector output
(b) phasemeter output.

The phasemeter output waveforms were observed to be identical from ping to ping. This indicates that the phase spikes are not caused by instrumentation errors arising from the phasemeter limiting on noise present at its inputs during nulls in the backscatter return. By observing the 316 kHz component of the received echo signals, it was established that the phase spikes reflect actual discontinuities in the phase of the receiver outputs. The phase discontinuities occurred at times during which the backscatter return was weak.

Reverberation arising from multipath propagation undergoes scattering from at least two surfaces. Consequently its amplitude is expected to be small in relation to that of the directly backscattered sound. Phase errors caused by multipath interference are only likely to occur therefore when the directly backscattered return grows weak. The phase discontinuities observed in the receiver outputs are consistent therefore with phase errors caused by multipath interference.

Multipath interference arising from reflection of sound at the water surface was eliminated as a possible interference source by disturbing the still water surface and observing any variation occurring in the receiver and phasemeter output waveforms. These remained identical from ping to ping. It was concluded that the receiver side baffle sufficiently shadowed the receivers from the water surface to enable surface multipath to be eliminated as an interference source.

It is believed that the phase discontinuities are caused by multipath interference arising from the scattering of sound from the tank back wall. This occurs as a result of the wide vertical beamwidth of the transmit array, the large receiver sidelobe level caused by reflection from the underside of the baffle and the proximity of the transducer arrays to the tank back wall. Unfortunately, time constraints did not allow for this to be verified experimentally.

4.2 Dam tests.

A fresh water dam whose bottom is known to consist of rocks embedded in fine mud was available for conducting further tests. The dam dimensions are approximately 60 m x 35 m x 7.5 m. A pontoon capable of being moved over the dam surface by means of tethered lines provided a convenient floating laboratory from which to conduct tests. Access to the water beneath the pontoon was provided by a rectangular slot cut into the pontoon floor. The floating laboratory is shown in Fig. 4.3.

Fig. 4.3 Photograph of floating laboratory.

The transmit and receive arrays together with their baffles were mounted on an Aluminium bracket. This is shown in Fig. 4.4. The bracket was adjusted for a transducer tilt angle of 45 degrees and clamped from the side of the pontoon access hole at a depth of 1 m. It should be noted that the receiver side baffle shown in Fig. 4.4 is an earlier version of that described in section 3.5 and was used only while mapping

the dam floor (see section 4.3). The directivity plots of this receiver baffle configuration were not as closely matched as those discussed in chapter 3 and are shown in appendix D.

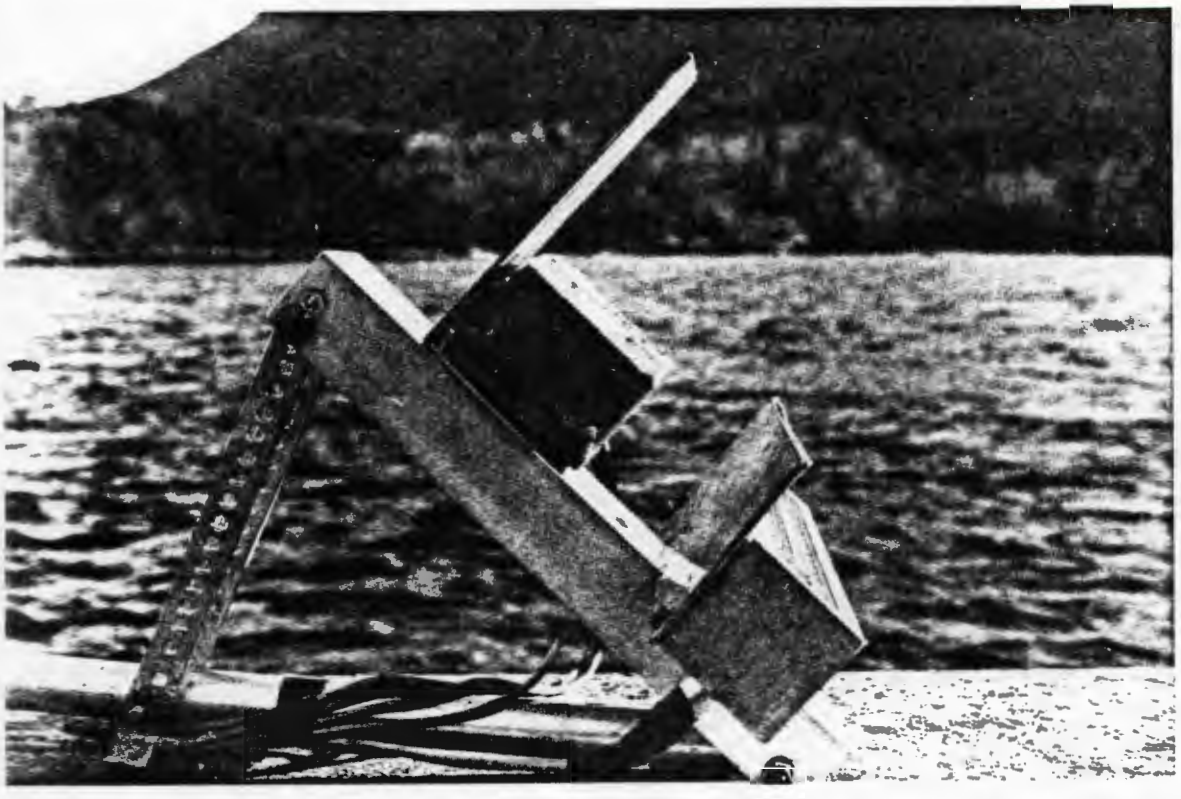

Fig. 4.4 Photograph of transducer arrays and side baffles on mounting bracket.

Multipath interference caused by scattering from the dam wall was avoided during tests by positioning the pontoon at a distance to the wall and ensuring that the transducer arrays were not directed perpendicularly to the wall. The position of the transducer arrays within the dam is shown in Fig. 4.5.

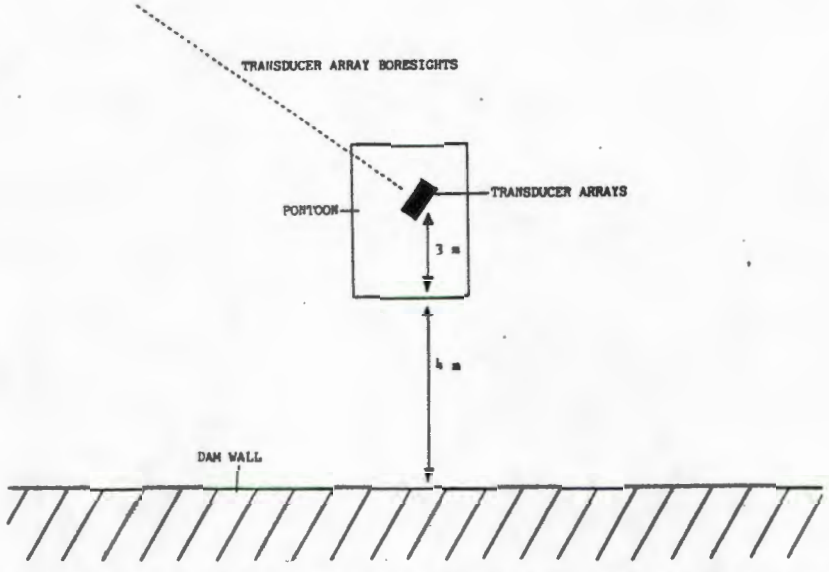

Fig. 4.5 Transducer array geometry during dam tests.

Phase discontinuities were once again apparent throughout each backscattered return. The envelope and phasemeter output waveforms for a typical echo return are shown in Fig. 4.6. Each waveform is sampled at 10 μs intervals over a slant range extending from 7.5 m to 15 m. The change in the slope of the phase ramp relative to the waveform shown in Fig. 4.2 is due to the receiver outputs driving the phasemeter being interchanged.

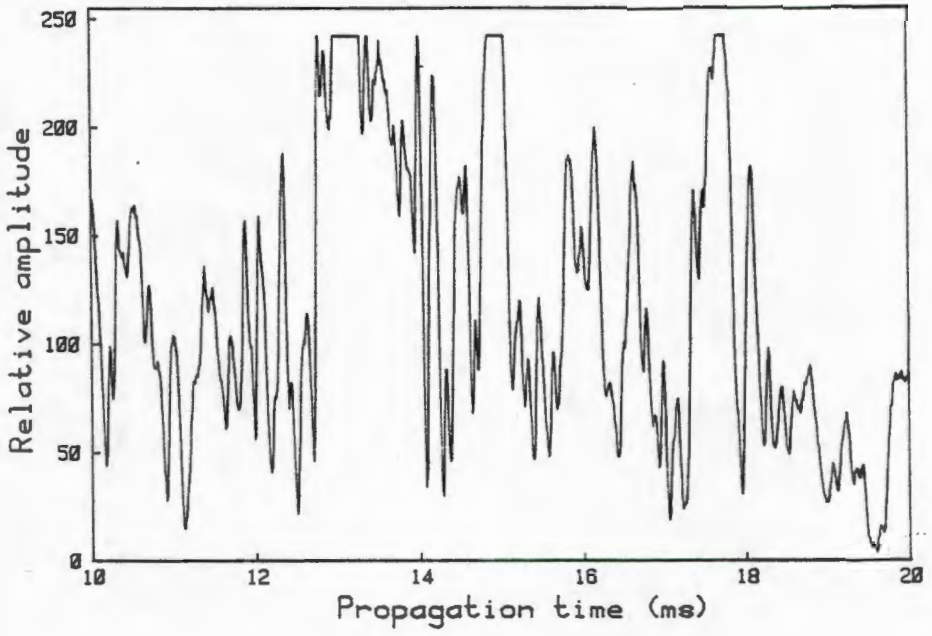

(a)

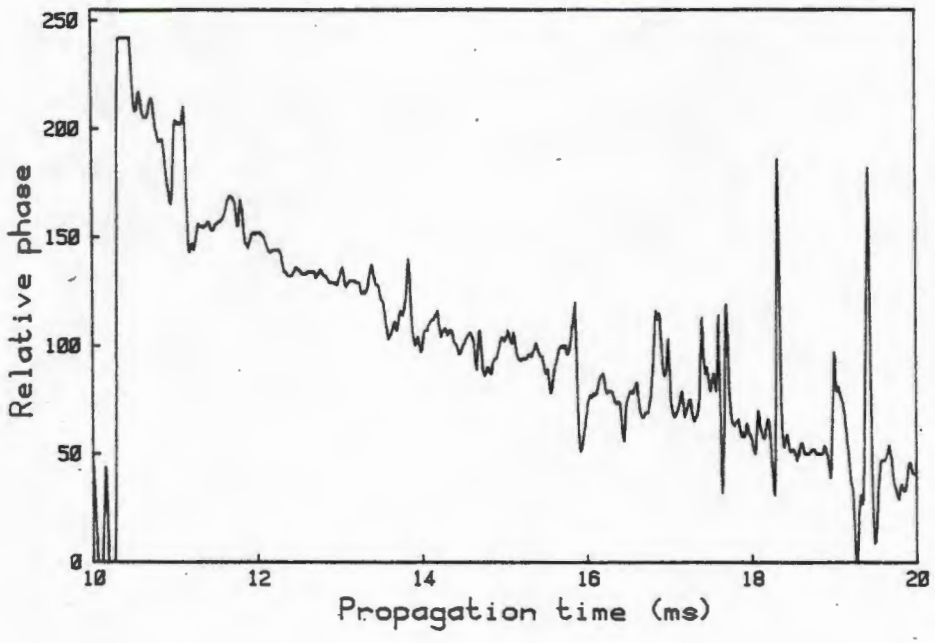

(b)

Fig. 4.6 Typical sonar waveforms recorded during dam tests
(a) envelope detector output
(b) phasemeter output.

The phase spikes occur at times during which the backscattered reverberation is weak. As indicated in the previous section, this is consistent with multipath interference. A baffle consisting of a closed cell foam material sandwiched between two wooden panels was used in an attempt to locate any interference paths at the dam site. This was done by placing the baffle at various positions in the immediate vicinity of the transducer arrays and observing any fluctuation occurring in the receiver and phasemeter outputs. No interference path capable of causing reverberation over the period during which the backscatter return occurred was found. It is evident that the interfering signal does not arise as a result of scattering from surrounding objects.

A possiblity not yet considered is that the multipath interference is caused by multiple scattering between feature on the dam floor. Additional insight into the manner in which sound is scattered from the dam floor was gained by conducting an experiment with a sidescan sonar with separated transducer arrays.

4.2.1 Experiment with a sidescan sonar with separated transducer arrays.

The 316 kHz transmit array of the bathymetric sidescan sonar system was used as a transmitter. A directive 9 element 185 kHz line array with a theoretical beamwidth of 1 degree was operated off resonance as a receiver. A large transmitter source level was used to ensure that the 316 kHz reverberation produced a sufficiently large signal at the 185 kHz array output. The transducer arrays were mounted on separate brackets and their azimuths adjusted until the transmit and receive beams coincided. The receiver was then rotated in the horizontal plane while its amplified output was observed on an oscilloscope.

Initially, the amplitude of the reverberation decreased with increasing angular separation. Beyond separations of 10 degrees however, the echo amplitude remained approximately constant with increasing angular offset. When the array beams were directed perpendicularly to each other, the echo amplitude was found to be 20 dB below that observed while aligned. This behaviour was repeatedly observed at all slant ranges during the echo return. An investigation with a baffle indicated that the reverberation was indeed caused by scattering from the dam floor.

The slow decrease in reverberation amplitude, observed with increasing angular offset between the transducer arrays, could be explained if the arrays were not directive. Both arrays are highly directive however and the slow decrease in reverberation level is not due therefore to acoustic energy radiated by the transmitter sidelobes. It was concluded that sound scattered by feature within the transmit beam is intercepted by scatterers within the receive beam and returned to the receivers. This is illustrated in Fig. 4.7.

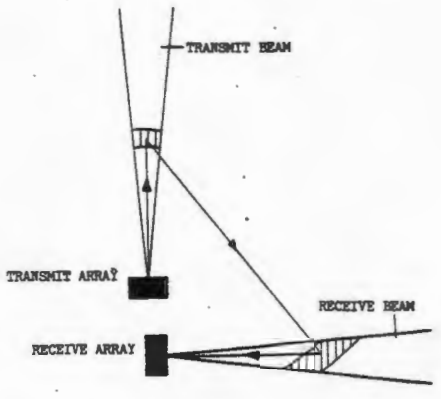

Fig. 4.7 Plan view of sound paths between transmit and receive beams.

The experiment described above indicates the existence of interference paths caused by multiple scattering of sound between feature on the dam floor. While the amplitude of the reverberation arising from each interference path is expected to be weak, due to the distribution of rocks over the dam

floor it is likely that a large number of interference paths exist at any moment in time. It is believed that the reverberation caused by multiple scattering from the dam floor is of sufficient magnitude to account for the phase discontinuities occurring at the receiver outputs during tests at the dam site. This suggests a fundamental problem with the bathymetric sidescan sonar system and is investigated in chapter 5.

4.3 Mapping of the dam floor.

This section describes the mapping of a 96 degree sector of the dam floor. Depth errors caused by phase spikes are decreased at the expense of reduced resolution by spatially averaging the digitized phase data.

The movement of the pontoon precluded its use as a stable platform from which to map the dam floor. Instead, the transducers were mounted from a stepper motor, attached to a bracket midway along the dam wall. The receive pre-amplifiers, beamformers and stepper motor control electronics were placed on the wall, while the remaining equipment was housed in the pontoon. Signals were conveyed between the dam wall and pontoon via coaxial cable. The equipment arrangement on the dam wall is shown in Fig. 4.8

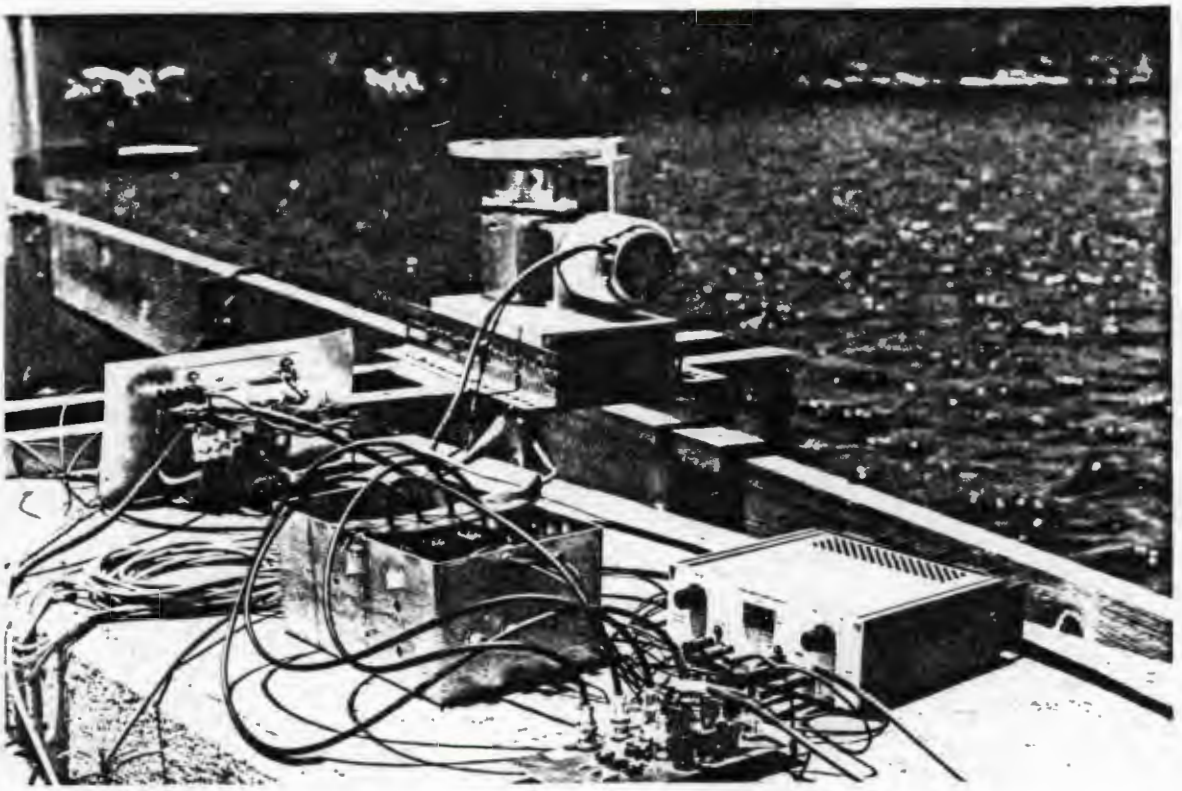

Fig. 4.8 Photograph of equipment arrangement on dam wall.

A polar scan of the dam floor was obtained by recording the phase waveforms occurring from 96 successive swaths, at angular increments of 1 degree, over a sector extending from 45 degrees to 141 degrees to the dam wall. The phasemeter output waveform corresponding to backscatter from each swath was captured and digitized at 10 μs intervals, over a slant range extending from 7.5 m to 15 m, by a Phillips PM 3055 digital storage oscilloscope. The digitized phase data was downloaded to a HP 85 microcomputer and stored on flexible disc for future processing. Data capture, storage and stepper motor positioning were carried out under computer control. The program listing is included in appendix C.

4.3.1 Results.

Computer processing of the data captured and stored at the dam site was performed on a HP 85 microcomputer.

The following processing steps were implemented:

1) Data compression.
2) Spatial averaging of phase data within a ping.
3) Spatial averaging of phase data from ping to ping.
4) Calculation of depth and horizontal range.
5) Polar to rectangular coordinate conversion.
6) Data conversion to format suitable for serial transfer to mainframe computer.

Compression and smoothing algorithms used during the computer processing are shown in appendix C. A software "lookup" table was used to relate the digitized phasemeter output to the corresponding declination angles. Its generation is described in appendix E.

After the transfer of the processed data to the UCT Sperry 1100 mainframe computer, the SACLANT resident graphics package was used to produce a 3-dimensional perspective picture of the dam floor. This is shown in Fig. 4.9.

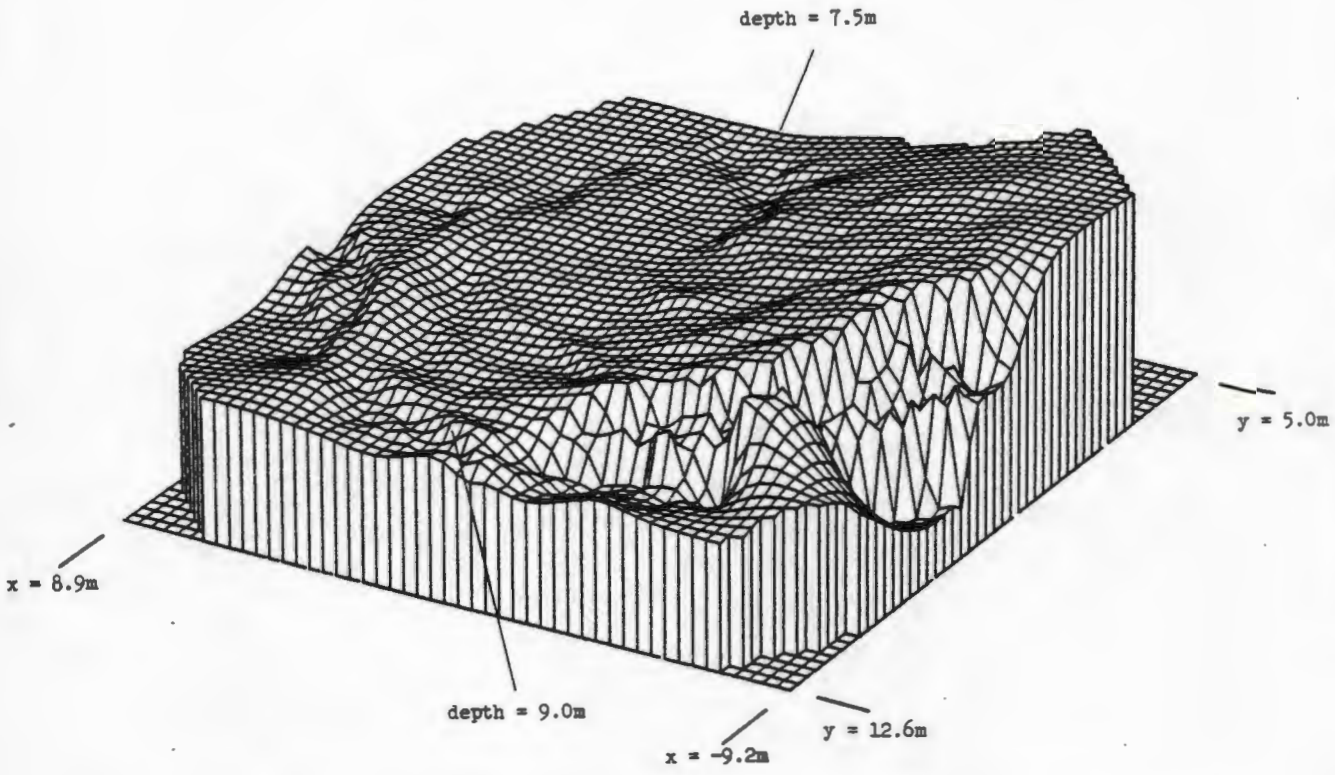

Fig. 4.9 3-dimensional perspective picture of dam floor.

The depth of the rectangular base on which the projection is drawn is 12 m. The dam floor is viewed looking towards the dam wall which runs along the x axis at y=0. The transducers are positioned at x=0, y=0. The dam floor is seen to slope gently upwards on either side of the transducer position and from a depth of approximately 7.3 m downwards to 9.0 m, away from the dam wall. The steep slope visible on the bottom right of the plot does not correspond to feature on the dam floor but is caused by backscatter originating from outside the unambiguous sector of the receivers.

A large amount of smoothing was implemented during processing of the phase data to ensure that depth errors were reduced to an acceptably low level. Unfortunately, this results in a sharp decrease in resolution. The dam floor is known to consist of a large number of rocks embedded in silt. No fine feature is however visible in the 3-dimensional picture.

While the loss of resolution is acceptable for certain applications such as contour mapping of the sea bed, it may be unacceptable in high resolution applications. If the high resolution capability of the bathymetric sidescan sonar system is to be fully realized, minimal smoothing should be applied to the phase data.

CHAPTER 5

MULTIPATH INTERFERENCE AND MULTIPLE SCATTERING

An experiment described in the previous chapter indicates that reverberation arising from multiple scattering between feature on the dam floor is of sufficient magnitude to cause substantial errors in the phase measurement performed by the receivers. This suggests a fundamental problem with the bathymetric sidescan sonar and is therefore sufficiently important to warrant a theoretical confirmation.

In this chapter, a mathematical model is developed enabling the ratio of the mean direct path reverberation intensity to the mean multipath reverberation intensity to be determined for an idealized sea bed. A statistical analysis of the direct path and multipath reverberation indicates that even at large mean interference ratios, a finite probability exists that the instantaneous amplitude of the multipath reverberation is sufficiently large to cause significant errors in the receiver phase measurement. A numerical evaluation of the mathematical model indicates that the receivers of the bathymetric sidescan sonar system are susceptible to phase error caused by multipath interference. Finally, an experiment is described in which reverberation caused by sound propagation over second order paths was observed.

5.1 Interference path geometry.

The interference paths discussed in this chapter are considered to arise as a result of secondary scattering of sound from the sea floor. While higher order scattering may cause multipath interference, the amplitude of the resultant reverberation is considered to be negligible in comparison to that produced by second order paths. Fig. 5.1 shows the geometry of a typical interference path.

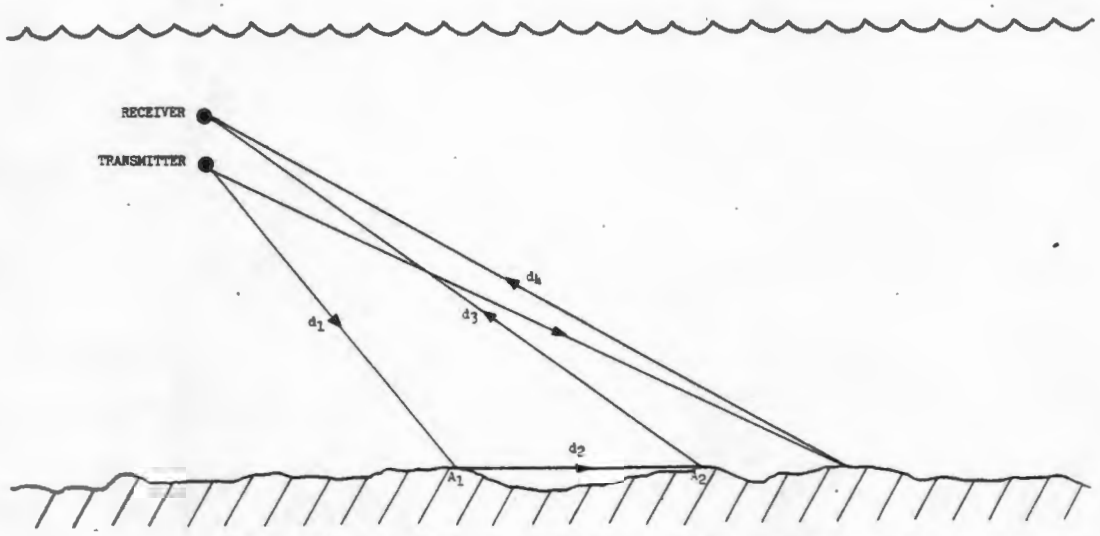

Fig. 5.1 Interference path geometry.

The acoustic energy scattered in the direction of A_2 by an area of sea bed A_1, is intercepted by A_2 and rescattered. The portion of this sound energy scattered in the direction of the receivers will interfere with a directly backscattered echo return originating from a slant range d_4

$$d_4 = \frac{d_1+d_2+d_3}{2}$$

Each scatterer pair produces two equal distance interference paths. These are the forward path transmitter-A_1-A_2-receiver and the reverse path transmitter-A_2-A_1-receiver. For reasons which become apparent in a later section, errors in the receiver phase measurement are assumed to occur as a result of reverberation arising from reverse scattering paths.

5.2 Phase errors introduced by multipath interference.

The reverberation caused by the interference paths described above introduce errors into the phase measurement performed by the receivers. To establish the magnitude of these errors, the interference situation shown in Fig. 5.2 is considered.

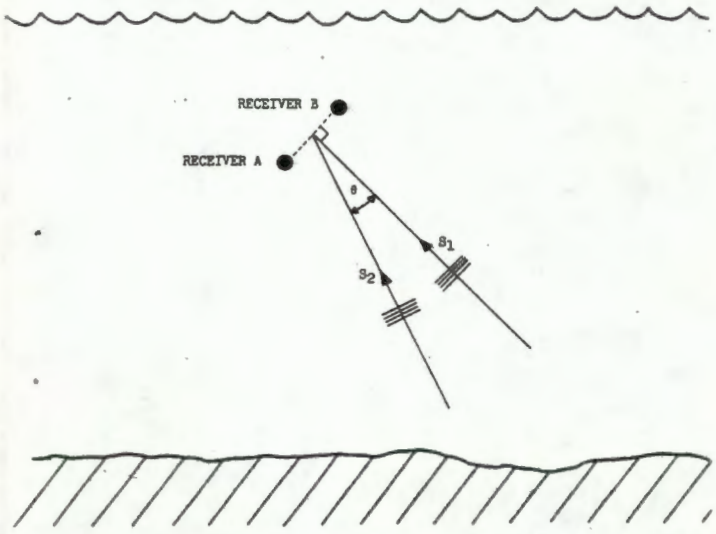

Fig. 5.2 Simultaneous reception of reverberation from differing declination angles.

A required directly backscattered signal S_1 is received simultaneously with an interference signal S_2 arriving from an elevation θ below S_1. For convenience the wanted signal S_1 is shown arriving along the receiver boresights. The phasor representation of the resulting receiver outputs R_A and R_B is shown in Fig. 5.3.

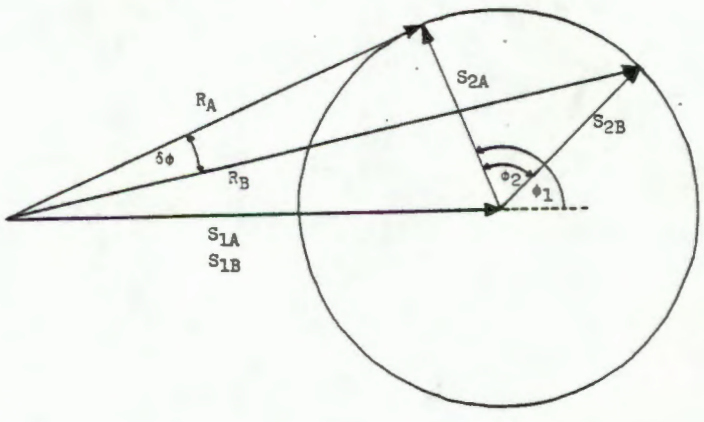

Fig. 5.3 Vector representation of receiver outputs showing phase error caused by interference signal.

As S_1 originates from along the receiver boresights, it introduces no phase shift between the receiver outputs. The arrival phase ϕ_1 depends on the precise difference in length between the direct and interference paths. If the difference in path length is Δd, then

$$\phi_1 = \frac{2\pi\Delta d}{\lambda}$$

At a frequency of 316 kHz a change in path length of 2.4 mm causes a phase shift of 180 degrees between the wanted and interference signals. ϕ_1 will fluctuate rapidly therefore as the direct path and interference paths change with time. As the arrival phase of the signals are unknown, the locii of the receiver outputs are shown.

A phase shift ϕ_2 is introduced by the difference in elevation angles from which S_1 and S_2 originate.

$$\phi_2 = \frac{2\pi d}{\lambda} \sin\theta$$

The interfering signal causes a phase error $\delta\phi$ in the receiver phase measurement. Fig. 5.4 shows phase error as a function of arrival phase, plotted for an interference signal originating from various declination angles. The amplitude of the interfering signal is assumed to be half that of the wanted signal.

It is evident that the phase errors introduced by multipath interference increase as the angular separation between the declination angles from which the direct path and multipath reverberation originate increases.

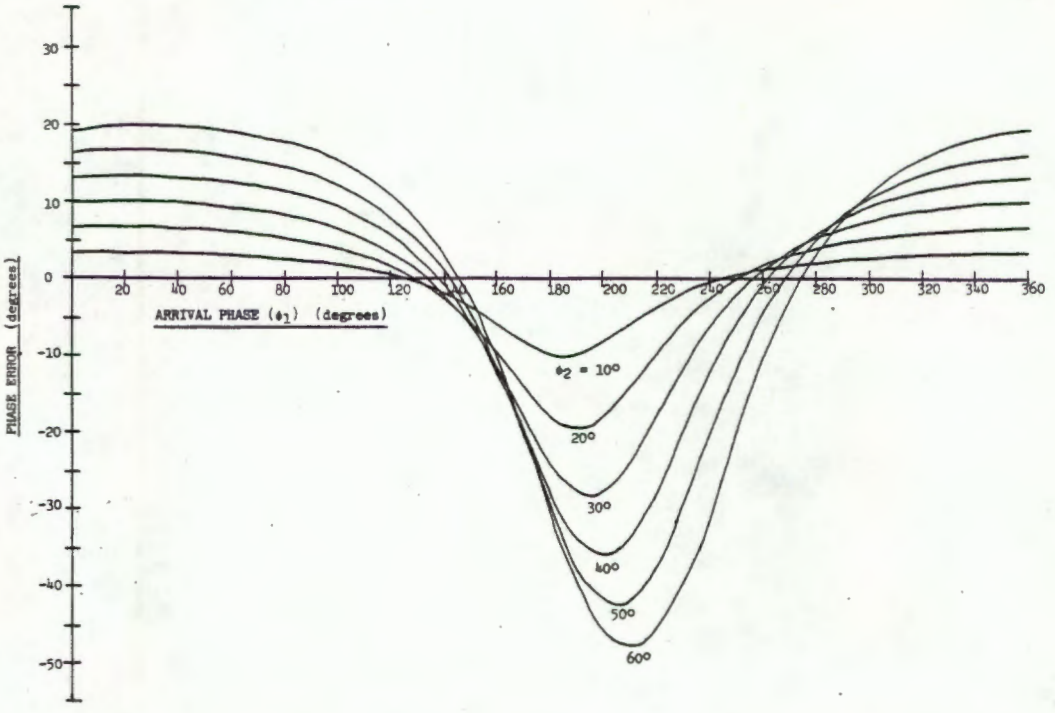

Fig. 5.4 Receiver phase error as a function of arrival phase.

5.3 Mathematical model of multipath interference.

A mathematical model enabling the ratio of the mean direct path reverberation intensity to the mean multipath reverberation intensity to be determined for a flat sea bottom, is developed by considering the scattering situation shown in Fig. 5.5.

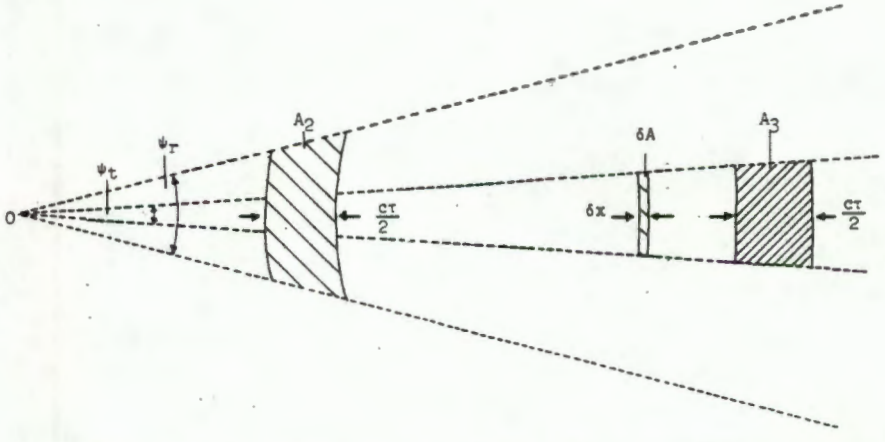

Fig. 5.5 Plan view of model geometry.

A transmitter and receiver situated at O uniformally illuminate a flat sea bed over a 90 degree vertical sector. At an instant in time, a sea bed area A_3 is insonified by the acoustic transmit pulse and returns direct path reverberation to the receivers. The sea bed area A_3 is a sector of an annulus centred about O and falling within the transmitter horizontal beamwidth ψ_t. The width of the annulus corresponds to the sonar resolution.

Simultaneously, an interference path caused by reverse scattering between sea bed areas δA and A_2, returns reverberation to the receivers. The sea floor area A_2 intercepting sound scattered by δA and returning reverberation to the receivers, is a portion of an annulus centred about δA and falling within the receiver horizontal beamwidth ψ_r. If the width δx of δA is infinitesimally small, the width of A_2 corresponds to the sonar resolution.

Assuming isotropic scattering to occur in the horizontal plane (Urick, 1960), the mean intensity i_m at the receivers of the reverberation arising from the single interference path described above is

$$i_m = \frac{I_o \delta A S_{f1} S_{f2} A_2}{d_1^2 d_2^2 d_3^2} \qquad (5.1)$$

where I_o is the transmitter source level, S_{f2} and S_{f1} are the bistatic scattering strengths arising at δA and A_2 respectively, d_1 and d_3 are the receiver and transmitter slant ranges to A_2 and δA respectively while d_2 is the separation between δA and A_2.

The elemental area δA insonified by the transmitter beamwidth is

$$\delta A = d_3 \psi_t \delta x \qquad (5.2)$$

If the width δx of δA is infinitesimally small, the sea bed area intercepting sound scattered from δA and returning reverberation to the receivers is approximately

$$A_2 = \frac{c\tau d_1 \psi_r}{2} \tag{5.3}$$

combining 5.2 and 5.3 with 5.1

$$i_m = \frac{I_o \psi_r \psi_t \delta x S_{f1} S_{f2} c\tau}{2 d_1^2 d_2 d_3} \tag{5.4}$$

It is evident that a large number of interference paths return reverberation to the receivers simultaneously with the sound directly backscattered from A_3. To determine the total intensity of the multipath reverberation at the receivers, it is assumed that an interference path exists for each elemental sea bed area at slant range d_3 smaller than the direct path slant range, such that

$$d_1+d_2+d_3 = 2d_4$$

The intensity I_m of the resultant reverberation is

$$I_m = \frac{I_o \psi_r \psi_t c\tau}{2} \int \frac{S_{f1} S_{f2}}{d_1^2 d_2 d_3} dx \tag{5.5}$$

where the integration is performed for each interference path within the transmitter and receiver vertical beamwidth.

The mean intensity I_d at the receivers of the direct path reverberation backscattered from A_3 is

$$I_d = \frac{I_o A_3 S_b}{d_4^4} \tag{5.6}$$

where S_b is the backscattering strength and d_4 is the direct path slant range.

Neglecting the effect of declination angle on the sea floor area insonified by the transmit pulse, the seabed area A_3 returning directly backscattered reverberation to the receivers is

$$A_3 = \frac{c\tau d_4 \psi_t}{2} \tag{5.7}$$

Combining 5.6 and 5.7

$$I_d = \frac{I_o c\tau \psi_t S_b}{2 d_4^3} \tag{5.8}$$

The linear mean interference ratio I_d/I_m is obtained by dividing 5.8 by 5.5.

$$\frac{I_d}{I_m} = \frac{S_b}{d_4^3 \psi_r \int \frac{S_{f1} S_{f2}}{d_1^2 d_2 d_3} dx} \tag{5.9}$$

The integral appearing in the above expression is not easily evaluated. It may however be approximated by a discrete summation performed at a sufficiently narrow strip width Δx. The interference ratio in the model becomes therefore

$$\frac{I_d}{I_m} = \frac{S_b}{d_4^3 \psi_r \sum \frac{S_{f1} S_{f2}}{d_1^2 d_2 d_3} \Delta x} \tag{5.10}$$

The above derivation has considered reverberation caused by reverse scattering from the sea floor. If the derivation is repeated for the forward path case, the identical expression is obtained. Due to the geometry of the flat sea floor model, the reverberation arising from the forward scattering paths originates from declination angles similar to that of the directly backscattered sound. Consequently, the errors introduced into the receiver phase measurement by forward path reverberation are small in relation to those caused by the reverse path reverberation. Multipath interference is therefore assumed to occur as a result of reverberation arising from reverse scattering paths.

5.4 Statistical analysis of instantaneous interference ratio

The direct and interference path signals fluctuate in time about their mean levels. Even if the ratio of mean wanted signal to mean interference signal is large, excessive error occurs in the receiver phase measurement when the direct path signal grows momentarily weak. It is therefore important that the probability of the interference path signal exceeding a particular fraction of the direct path signal amplitude be determined.

Based upon the Central Limit theorem, the backscattered reverberation may be expected to satisfy Gaussian statistics (Burdic, 1984), (Cron and Schumacher, 1961). Consequently, the envelope of the backscattered sound is described by a Rayleigh random variable, satisfying a probability density function of the form

$$q(A) = \frac{A}{\sigma^2} \exp\left(-\frac{A^2}{2\sigma^2} \right)$$

The Central Limit theorem may similarly be used to ascribe Gaussian statistics to the reverberation caused by multiple scattering from the sea bed. Its envelope too is therefore described by a Rayleigh random variable, satisfying a probability density of the above form.

If $q_d(A)$ and $q_m(A)$ are the respective probability density functions of the direct path and multipath reverberation envelopes, with means σ_d and σ_m, the probability of the magnitude of the multipath interference signal exceeding a fraction x of the direct path signal amplitude is determined below. This is illustrated in Fig. 5.6 which shows typical Rayleigh probability density functions for the direct path and multipath reverberation envelopes.

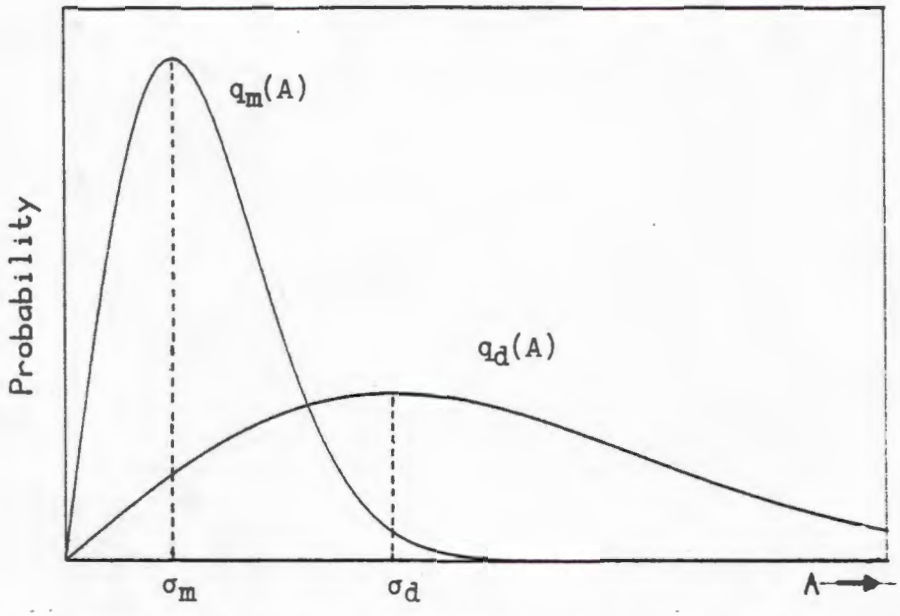

Fig. 5.6 Typical Rayleigh probability density functions of direct path and multipath reverberation envelopes.

The following analysis is an extension of a derivation by Denbigh.

Probability that the direct path reverberation assumes a value between a and a+da

$$q_d(a)da \tag{5.11}$$

Probability that the amplitude of the reverberation due to multipath interference excedes xa

$$\int_{xa}^{\infty} q_m(A)dA \tag{5.12}$$

Joint probability that the direct path reverberation assumes an amplitude between a and a+da, and the multipath reverberation exceeds xa

$$q_d(a)da \int_{xa}^{\infty} q_m(A)dA \tag{5.13}$$

Probability that the direct path reverberation assumes any amplitude and the multipath interference exceeds a fraction x of this value

$$= \int_0^\infty q_d(a) \int_{xa}^\infty q_m(A)dA\ da$$

$$= \int_0^\infty \frac{a}{\sigma_d^2} \exp(-\frac{a^2}{2\sigma_d^2}) \int_{xa}^\infty \frac{A}{\sigma_m^2} \exp(-\frac{A^2}{2\sigma_m^2})dA\ da$$

$$= \int_0^\infty \frac{a}{\sigma_d^2} \exp(-\frac{a^2}{2}\{\frac{1}{\sigma_d^2} + \frac{x^2}{\sigma_m^2}\})da$$

$$= \frac{\sigma_m^2}{\sigma_m^2+x^2\sigma_d^2} \qquad (5.14)$$

The above relationship is plotted for various values of x in Fig. 5.7. It indicates that while a finite probability exists that the amplitude of the multipath reverberation exceeds a significant proportion of the direct path reverberation amplitude at all mean interference ratios, this probability rapidly decreases with increasing mean interference ratio.

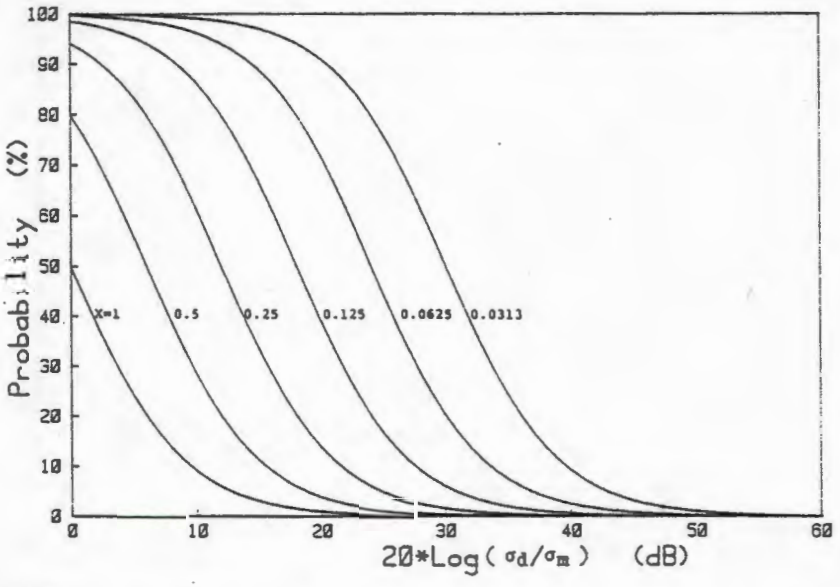

Fig. 5.7 Graph showing probability of multipath reverberation exceeding various fractions of direct path reverberation amplitude.

5.5 Scattering of sound from the sea floor.

The magnitude of the multipath reverberation is dependent on the proportion of sound scattered at small grazing angles by the sea floor. A brief examination of the manner in which sound is scattered by the sea floor follows.

The fundamental ratio governing the manner in which sound incident on the sea floor is redistributed throughout the water volume by scattering, is the bottom scattering strength S_s. It is defined as being the ratio of sound intensity I_s, scattered by a unit area, referred to a distance of 1 m, to the incident plane wave intensity I_i (Urick, 1975).

$$S_s = 10 \log \frac{I_s}{I_i}$$

While a relatively large number of mostly discordant measurements of acoustic backscattering from the sea bed have been reported in the literature, the bistatic case in which the receiver and transmitter are separate has received little attention.

Urick and Saling (1962), Mackenzie (1961), and others have suggested that the scattering strength of the sea bed may be expressed in the form

$$S_s = \mu_k \sin\theta_i \sin^{k-1}\theta_s$$

where μ_k is a constant of proportionality, while θ_i and θ_s are the grazing angles of the incident and scattered sound respectively. When k=1 the scattering strength exhibits no dependence on θ_s. This corresponds to the case of omnidirectional scattering. k=2 corresponds to perfectly diffuse Lambert scattering and is likely to occur from bottoms having significant roughness relative to the wavelength of the incident sound.

Unfortunately, experimental verification of the above approximation at small grazing angles has been restricted to the monostatic case for which $\theta_i = \theta_s$. The backscattering strength may be expressed in the form

$$S_b = \mu_k \sin^k \theta_b$$

where θ_b is the grazing angle of the backscattered sound and S_b is the backscattering strength (Wong and Chesterman, 1968).

A number of investigations into the validity of the above approximation have been conducted for grazing angles varying between 10 degrees to 90 degrees. Several studies have favoured the case k=2 corresponding to diffuse Lambert scattering (Urick, 1954), while others have favoured the omnidirectional case k=1 (Mackenzie, 1961).

Wong and Chesterman conducted measurements designed to study the backscattering behaviour of shallow coastal sea bottoms at grazing angles approaching grazing incidence (Wong and Chesterman, 1968). They conclude that at very small grazing angles (between 0.5 and 6 degrees), the backscattering strength is constant (k=0). At a few geographical locations however, a weak angular dependence corresponding to small k values was observed as the grazing angles approached grazing incidence.

This behaviour is confirmed by McKinney and Anderson (1964), who observed a slight increase in backscattering strength at grazing angles below 2 degrees as the grazing angle was further decreased. Fig. 5.8 shows the backscattering strength of a number of bottom types plotted against grazing angle. The bottom types corresponding to the symbols are described in Table 1.

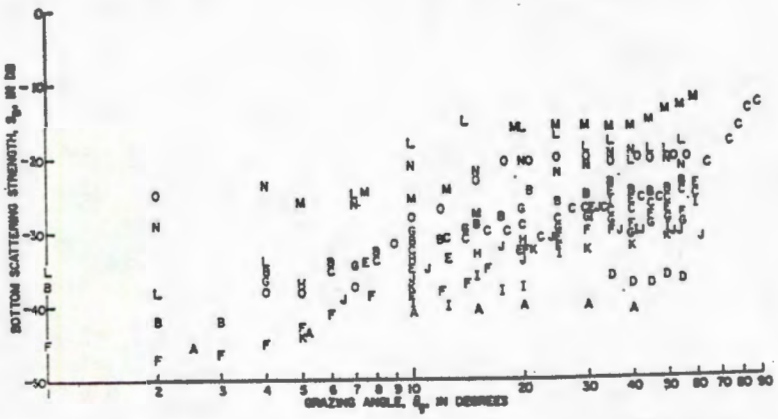

Fig. 5.8 Bottom backscattering strength as a function of grazing angle.
(From McKinney and Anderson, 1964)

Area	Sediment description
A	Fine sandy mud
B	Medium sandy clay
C	Muddy fine sand
D	Very fine sandy mud
E	Silty fine sand
F	Clayey medium sand
G	Muddy fine sand
H	Mud–Sand
I	Sand
J	Medium sand
K	Medium sand
L	Sandy pebble gravel
M	Sandy pebble gravel
N	Solid rock
O	Solid coral, huge chunks coral growth

Table 1 Description of bottom type.
(From McKinney and Anderson,1964)

The reverberation from each interference path is twice scattered by the sea floor. Consequently, its amplitude is small in relation to that of the directly backscattered sound. Considerable interference is therefore only likely to occur, when the directly backscattered reverberation grows weak. The backscattering strength data presented in Fig. 5.8 indicates an increase in backscattering strength of almost 20 dB as the ocean bottom changes from sand through pebble to rock. Large receiver phase errors are likely to occur therefore when the multipath reverberation arises as a result of scattering between prominent feature such as rock, while the direct path reverberation is returned by mud or sand portions of the sea floor.

5.6 Numerical evaluation of mathematical model.

The interference ratio

$$\frac{I_d}{I_m} = \frac{S_b}{d_4^3 \psi_r \sum \frac{S_{f1} S_{f2}}{d_1^2 d_2 d_3} \Delta x}$$

is evaluated by dividing the idealized sea bed into a number of small strips, each of width Δx and determining the path parameters d_1, d_2, d_3 corresponding to each strip. The geometries and path parameters of the forward and reverse path models are shown in appendix F.

To determine the direct path to multipath interference ratio likely to be encountered during operation of the bathymetric sidescan sonar system, the expression for interference ratio in the model is numerically evaluated for a sea bottom at a depth of 30 m and a direct path echo originating from a declination angle of 45 degrees at a slant range of 42.43 m. The ocean bottom consists of rock and fine silty mud. A receiver beamwidth of 10 degrees is assumed.

The sea floor is divided into a number of 1 m wide strips. This is sufficiently narrow to ensure that the intensity of the multipath reverberation is approximately constant over each strip. The multipath reverberation from alternate sea bed strips is assumed to occur as a result of scattering between rocks and the remainder between mud. The interference ratio is determined at a moment during which the directly backscattered reverberation is returned by a mud portion of the sea floor. Due to the unavailability of suitable experimental data on bistatic scattering strengths, the monostatic backscattering data presented in Fig. 5.8 was used to determine the following values for S_b, S_{f1} and S_{f2}.

S_b = -41 dB (mud)
$S_{f1} = S_{f2}$ = -46 dB (mud)
$S_{f1} = S_{f2}$ = -29 dB (rock)

An experiment described in appendix G, indicates that the intensity of sound scattered from a rough surface at small grazing angles increases as the grazing angle of the incident sound increases. It is believed therefore, that the use of monostatic scattering strength data to determine numerical values for S_{f1} and S_{f2} , results in a conservative estimate of multipath reverberation intensity. At the same time however, it should be noted that the data presented in Fig. 5.8, was determined from measurements conducted at a frequency of 100 kHz. At the 316 kHz operating frequency of the bathymetric sidescan sonar, decreased penetration of sound into the mud bottom will occur and consequently, the intensity of the direct path reverberation will be slightly larger than predicted. These effects will tend to cancel and the resulting interference ratio is believed to provide a reasonably accurate indication of the multipath interference likely to be encountered in a real sonar enviroment.

The reverse path model parameters for the interference situation described above, are shown in Table 2. The path parameters are calculated for the centre of each strip. The difference in elevation between the seabed areas from which the direct path and multipath reverberation originate are also indicated.

n	Strip type	d_1 (m)	d_2 (m)	d_3 (m)	θ (degrees)	$\frac{S_{f1} S_{f2}}{d_1 d_2^2 d_3} \Delta x$
1	rock	40.51	2.27	42.07	2.8	2.88×10^{-11}
2	sand	37.53	5.95	41.38	8.1	1.15×10^{-14}
3	rock	35.34	8.83	40.70	13.1	1.42×10^{-11}
4	sand	33.71	11.12	40.03	17.9	3.78×10^{-15}
5	rock	32.51	12.98	39.37	22.3	7.35×10^{-12}
6	sand	31.62	14.51	38.73	26.6	2.45×10^{-15}
7	rock	30.98	15.77	38.11	30.6	5.40×10^{-12}
8	sand	30.53	16.83	37.50	34.3	1.94×10^{-15}
9	rock	30.24	17.71	36.91	37.8	4.53×10^{-12}
10	sand	30.07	18.46	36.34	41.1	1.70×10^{-15}
11	rock	30.00	19.08	35.78	45.0	4.06×10^{-12}

Table 2 Reverse path model parameters.

While interference paths with a small separation between primary and secondary scatterers produce large reverberation levels, these originate from declination angles similar to that of the backscattered sound and cause negligible phase error. Considering therefore, only the reverberation originating from elevation angles greater than 18 degrees from the backscattered sound, the summation

$$\sum_{n=4}^{11} \frac{S_{f1} S_{f2}}{d_1 d_2^2 d_3} \Delta x = 2.13 \text{ E-11}$$

The interference ratio in the model is

$$10 \log \left(\frac{7.9 \text{ E-5}}{42.43^3 \times 0.175 \times 2.13 \text{ E-11}} \right)$$

$= 24$ dB.

5.6.1 Discussion.

The rock and mud sea bottom used in the numerical evaluation of the model interference ratio, corresponds to that of the dam site at which field tests were conducted. The resulting mean interference ratio of 24 dB is extremely low and consequently, the probability of the amplitude of the multipath reverberation exceeding large fractions of the direct path reverberation amplitude is high. This is indicated in Table 3, which shows the probability of the amplitude of the multipath reverberation exceeding various fractions x, of the direct path reverberation amplitude. The maximum phase and depth errors caused by the relevant instantaneous interference amplitudes are also indicated. A receiver system capable of operation over a ±26 degree sector is assumed, while depth errors are calculated at a slant range of 42 m.

x	Probability (%)	Maximum phase error (degrees)	Maximum depth error (m)
0,125	20,3	14,3	1,5
0,250	6,0	28,1	3,0
0,500	1,6	53,1	5,7

Table 3 Error probabilities for a mean interference intensity ratio of 24 dB.

In the numerical evaluation of interference ratio shown in section 5.6, only multipath reverberation originating from elevation angles greater than 18 degrees from the backscattered sound was considered. Consequently, the actual errors introduced into the receiver phase measurement, when the amplitude of the multipath reverberation exceeds the indicated fractions of the direct path reverberation amplitude, are, subject to variations in arrival phase, similar to the maximum phase errors shown in Table 3. The numerical evaluation of the interference ratio indicates

therefore, that the receiver system of the bathymetric sidescan sonar is susceptible to interference caused by the multiple scattering of sound from the sea floor.

The expression for the interference ratio in the model, indicates that the bathymetric sidescan sonar may be made less susceptible to interference by reducing the horizontal beamwidths of the receivers. If the numerical evaluation shown in section 5.6 is repeated, assuming a receiver beamwidth of 1 degree, the model interference ratio increases to 34 dB. The resulting increase in mean interference ratio results in a sharp decrease in the probability of phase error. This is indicated in Table 4.

x	Probability (%)	Maximum phase error (degrees)	Maximum depth error (m)
0,125	2,5	14,3	1,5
0,250	0,6	28,1	3,0
0,500	0,2	53,1	5,7

Table 4 Error probabilities for a mean interference intensity ratio of 34 dB.

Typically, the sea floor over which a bathymetric sidescan sonar might operate, consists of sand and rock. Decreased penetration of sound occurs into the sand bottom. Consequently, the amplitude of the backscattered reverberation is likely to be significantly greater than for the mud bottom. If the numerical evaluation shown in section 5.6 is repeated for a sand and rock bottom, assuming a receiver beamwidth of 1 degree, the interference ratio increases to 45 dB. At this large mean interference ratio, the probability of significant errors occurring in the receiver phase measurement becomes diminishingly small. This is indicated in Table 5.

x	Probability (%)	Maximum phase error (degrees)	Maximum depth error (m)
0,125	0,20	14,3	1,5
0,250	0,05	28,1	3,0
0,500	0,01	53,1	5,7

Table 5 Error probabilities for a mean interference intensity ratio of 45 dB.

5.7 Observation of reverberation caused by secondary scattering from a model surface.

Reverberation caused by secondary scattering from a model surface was observed by conducting an experiment in the water tank at the Central Acoustics Laboratory, UCT.

Secondary scattering paths were created by forming primary and secondary groups of scatterers from irregular lumps of Polystyrene, bonded to a smooth Aluminium base. The Aluminium base specularly reflects incident sound, thereby ensuring that reverberation observed at the receiver is due mainly to scattering from the Polystyrene scatterers. The scattering surface is shown in Fig. 5.9.

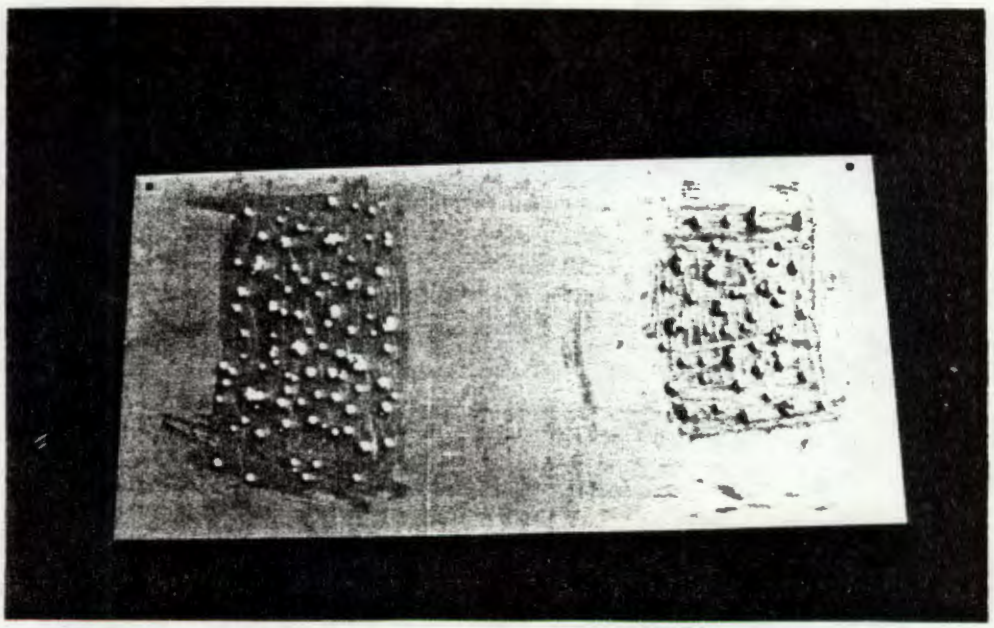

Fig. 5.9 Photograph of Aluminium base showing primary and secondary groups of Polystyrene scatterers.

The scattering surface was suspended against a tank wall and the primary scatterer group insonified by an acoustic source, producing 5 μs, 4.5 MHz sinusoidal pulses, at a grazing angle of 60 degrees and a slant range of 200 mm. The receiver was positioned at a slant range of 500 mm from the secondary scatterer group and directed to receive forward scattered sound, intercepted and rescattered by the secondary scatterers. Direct insonification of the secondary scatterers by the transmit beam, was avoided by introducing an Aluminium baffle between the acoustic source and the secondary scatterers. The baffle was carefully positioned to minimize diffraction effects caused by the baffle edge. The backscattered echo amplitude was determined by shifting the transmitter position, without altering its slant range or grazing angle, to directly insonify the secondary scatterer group. Fig. 5.10 indicates the transmitter position, relative to the scatterers, for the two measurements.

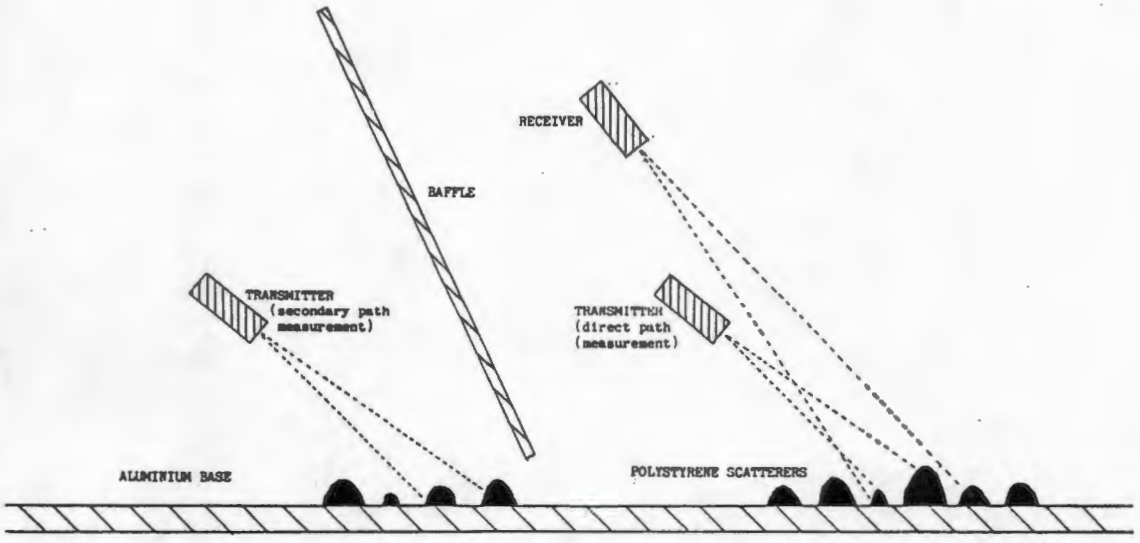

Fig. 5.10 Transducer positions during direct and secondary path measurements.

The direct path is shorter than the secondary path. As the scatterer separation is small relative to the total path length, the error introduced is small and was neglected. A photograph of the experimental arrangement in the water tank during the secondary scattering measurement is shown in Fig. 5.11.

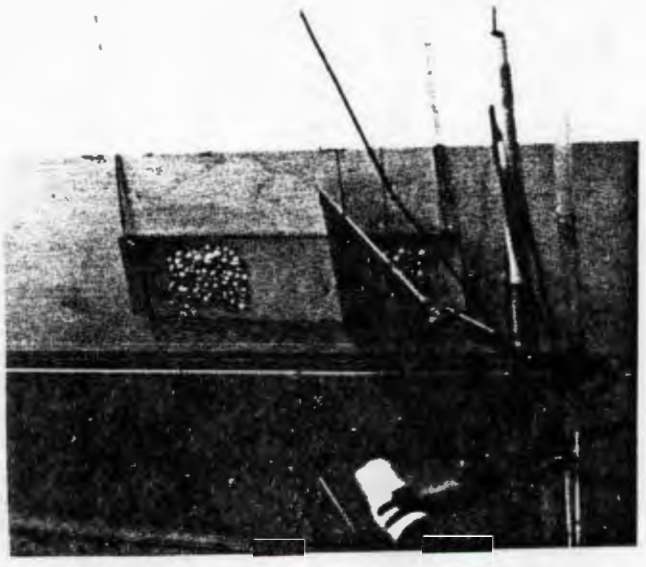

Fig. 5.11 Experimental arrangement in water tank during forward path measurement.

Typical receiver outputs due to reverberation caused by the propagation of sound over the forward path and the direct path are shown in Fig. 5.12. The resulting mean interference ratio is 26 dB.

Oscilloscope settings:
10 μs/div, 1 mV/div.
(a)

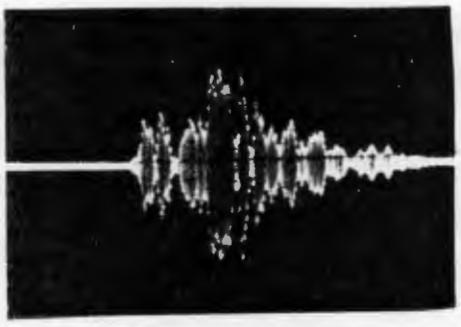

Oscilloscope settings:
10 μs/div, 20 mV/div.
(b)

Fig. 5.12 Typical receiver outputs (a) forward path (b) direct path.

The mathematical model previously developed, assumed the intensity of the multipath interference to decrease with the square of the scatterer separation. This behaviour was confirmed by mounting the scatterer groups on separate bases and observing the decrease in the amplitude of the secondary path reverberation, as the scatterer separation was increased. A decrease of 8 dB occurred when the scatterer separation was doubled from 100 mm to 200 mm. This is in close agreement with the 6 dB decrease predicted by the increased transmission loss introduced by spherical spreading of the sound.

CHAPTER 6

CONCLUSIONS

The construction of a bathymetric sidescan sonar system capable of operation over a 39 degree vertical sector has been described.

Tests conducted at a dam site indicate that the completed sonar system does not operate as required. Discontinuities present in the receiver phase measurement do not correspond to features on the dam floor and cause errors in the depth profiles produced by processing the sonar phase data.

A sector of the dam floor was mapped by the bathymetric sidescan sonar and a 3-dimensional perspective picture presented. Since phase spikes had to be reduced to an acceptable level by smoothing, the picture exhibits a disappointing resolution, much poorer than that corresponding to the sonar pulse width.

An experiment conducted using a sidescan sonar with separated transducer arrays indicates that these phase errors are caused by reverberation, resulting from the multiple scattering of sound by the dam floor.

A theoretical confirmation was obtained by constructing a mathematical model, enabling the ratio of the mean intensity of the direct path reverberation to the mean intensity of the multipath reverberation to be determined for an idealized sea bed.

An evaluation of the model indicates that the intensity of the multipath reverberation occurring at the dam site is sufficiently large to account for the phase discontinuities observed during field tests.

Based upon this model, the following recomendations are made so that future systems will be less susceptible to interference :

1. The receiver horizontal beamwidth should be reduced. This is because the model indicates that the intensity of the multipath reverberation is proportional to the horizontal receiver beamwidth. A substantial reduction in interference is achieved by using receivers which are highly directive in the horizontal plane. The receivers used in the present system produce a horizontal beamwidth of 10 degrees. If the receiver beamwidth is decreased to 1 degree, a 10 dB reduction in the mean intensity of the multipath reverberation is achieved.

2. A second side baffle should be positioned to shadow the receivers from the sea floor area outside their unambiguous sector. This is because the reflection of sound from the underside of the receiver baffle results in the receivers exhibiting large sidelobes in the direction of the sea floor. Consequently, the receivers are susceptible to interference originating from outside of their unambiguous sector.

In concluding, it should be noted that due to the statistical nature of reverberation, it is not possible to completely eliminate receiver phase errors caused by multipath interference. It is believed however, that the measures suggested above will result in a sufficiently large reduction in the mean amplitude of the multipath signal to ensure that the probability of significant errors occurring in the receiver phase measurement will be small. The decreased probability of phase error will enable depth profiles to be produced with minimal smoothing of the sonar phase data. Consequently, a resolution approaching that corresponding to the transmit pulse width may be achieved, allowing the high resolution capability of the bathymetric sidescan sonar to be more fully realized.

CHAPTER 7

REFERENCES

Burdic, W.S., Underwater acoustic system analysis, Prentice-Hall Inc., New Jersey, 1984.

Cron, B.F. and Schumacher, W.R., Theoretical and experimental study of underwater sound reverberation, J. Acoust. Soc. Am., pp.881-888, 1961.

Denbigh, P.N., The design of sidescan arrays and the elimination of vertical sidelobes, Institute of Acoustics Specialist Meeting on Transducer Arrays and Array Processing, pp.11-18, 1978.

Denbigh, P.N., A bathymetric sidescan sonar, Ultrasonics International 79 Conference Proceedings, Graz, pp.321-326, 1979.

Denbigh, P.N., Glint and its effect on the accuracy of a sea bed profiling sonar, Institute of Acoustics Conference on Signal Processing in Underwater Acoustics, Loughborough, pp.7.1-7.8, 1980.

Denbigh, P.N., Stereoscopic visualization and contour mapping of the sea bed using a bathymetric sidescan sonar (BASS), Radio and Electronic Engineer, pp.301-303, 1983.

Hood, C.R., A simple form of construction for multi-element arrays, MAFF Fisheries Laboratory, Lowestoft.

Hung, B. and Goldstein, A., Acoustic parameters of commercial plastics, IEEE Trans. on Sonics and Ultrasonics, pp.249-254, 1983.

Mackenzie, K.V., Bottom reverberation for 530- and 1030-cps sound in deep water, J. Acoust. Soc. Am., pp.1498-1504, 1961.

Mackenzie, K.V., Long-range shallow water bottom reverberation, J. Acoust. Soc. Am., pp.62-66, 1962.

McKinney, C.M. and Anderson, C.D., Measurements of backscattering of sound from the ocean bottom, J. Acoust. Soc. Am., pp.158-163, 1964.

Roy, S., Minimization of mutual coupling in transducer arrays, First South African Congress on Acoustics Conference Proceedings, Pretoria, 1985.

Runciman, P., A three dimensional imaging sonar, UCT Masters Thesis, Dept. of Electrical and Electronic Engineering, 1986.

Schmidt, P.B., Monostatic and bistatic backscattering measurements from the deep ocean bottom, J. Acoust. Soc. Am., pp.326-331, 1971.

Smith, S.W. et al, Angular response of Piezoelectric elements in phased array ultrasound scanners, IEEE Trans. on Sonics and Ultrasonics, pp.185-191, 1979.

Urick, R.J., the backscattering of sound from a harbour bottom, J. Acoust. Soc. Am., pp.231-235, 1954.

Urick, R.J., Side scattering of sound in shallow water, J. Acoust. Soc. Am., pp.351-355, 1960.

Urick, R.J., Principles of underwater sound, McGraw-Hill Inc., 1975.

Weintroub, J., Fish stock assessment by a statistical analysis of echo sounder signals, UCT Masters Thesis, Dept. of Electrical and Electronic Engineering, 1986.

Wong, H., Bottom backscattering near grazing incidence in shallow water, J. Acoust. Soc. Am., pp.1713-1718, 1968.

APPENDIX A

CIRCUIT DIAGRAMS

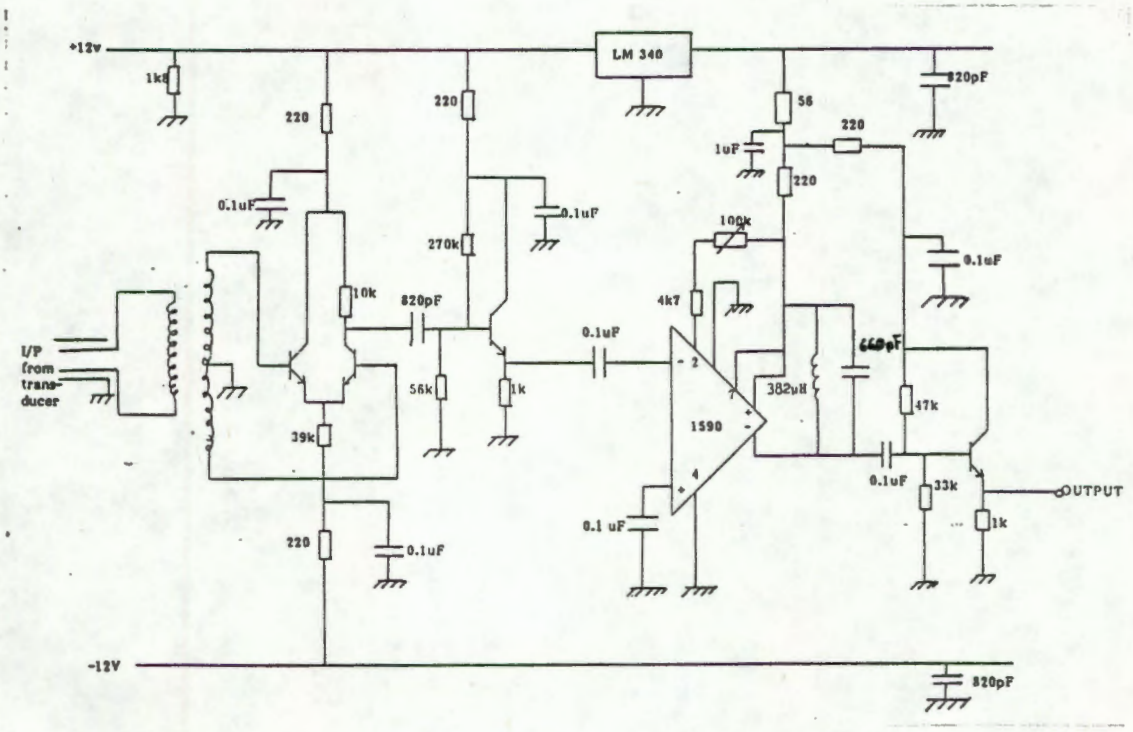

Fig. A.1 Circuit diagram of tuned receiver preamplifier. (Nominal voltage gain = 60 dB, centre frequency = 316 kHz, Q = 28). Preamplifier designed by Runciman (1986). Circuit diagram from Weintroub (1986).

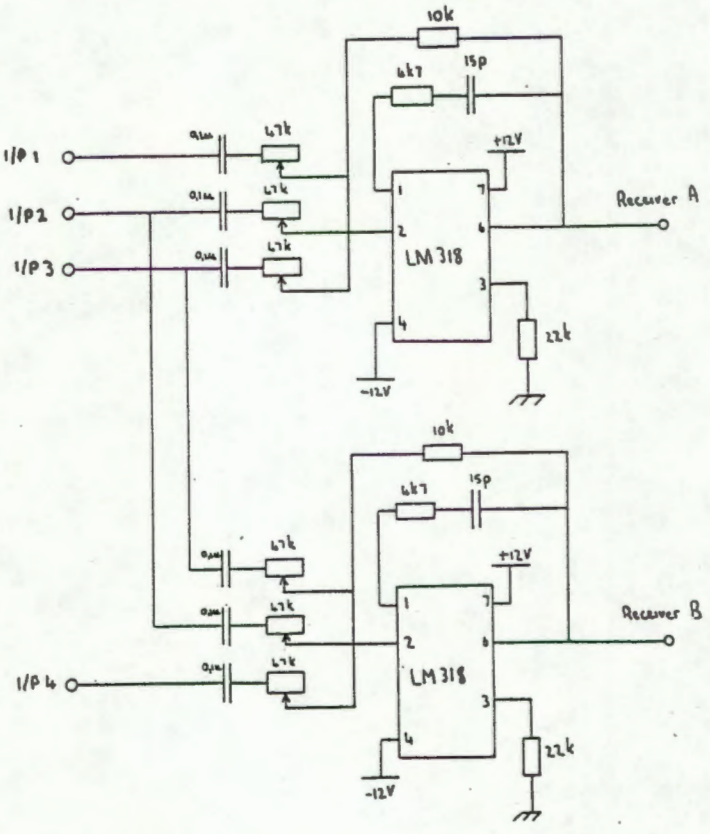

Fig. A.2 Circuit diagram of receiver beamformers.

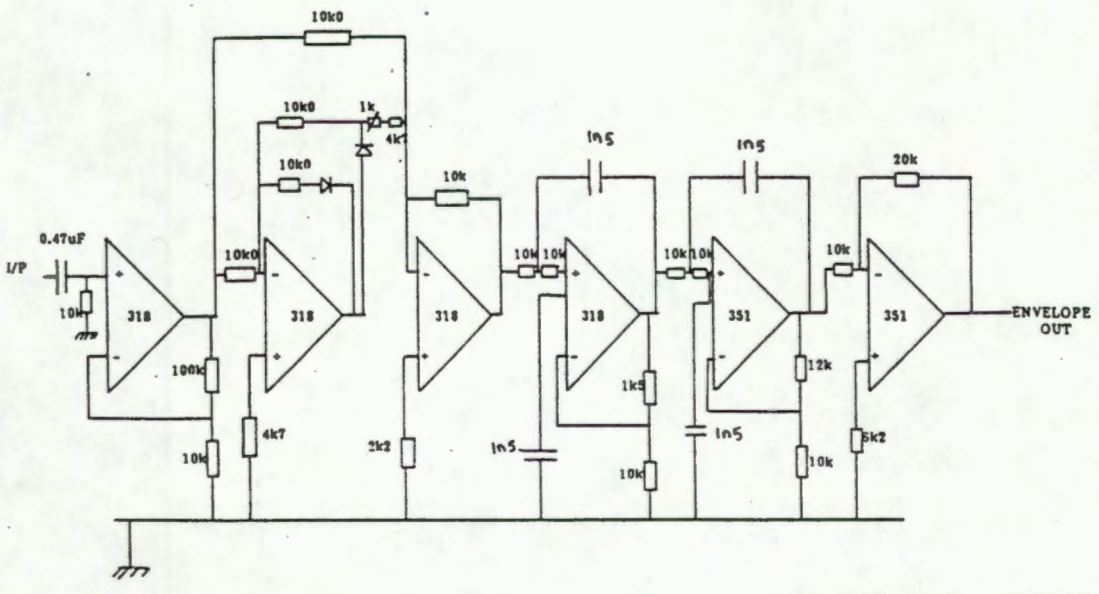

Fig. A.3 Precision envelope detector circuit.
(from Weintroub, 1986).

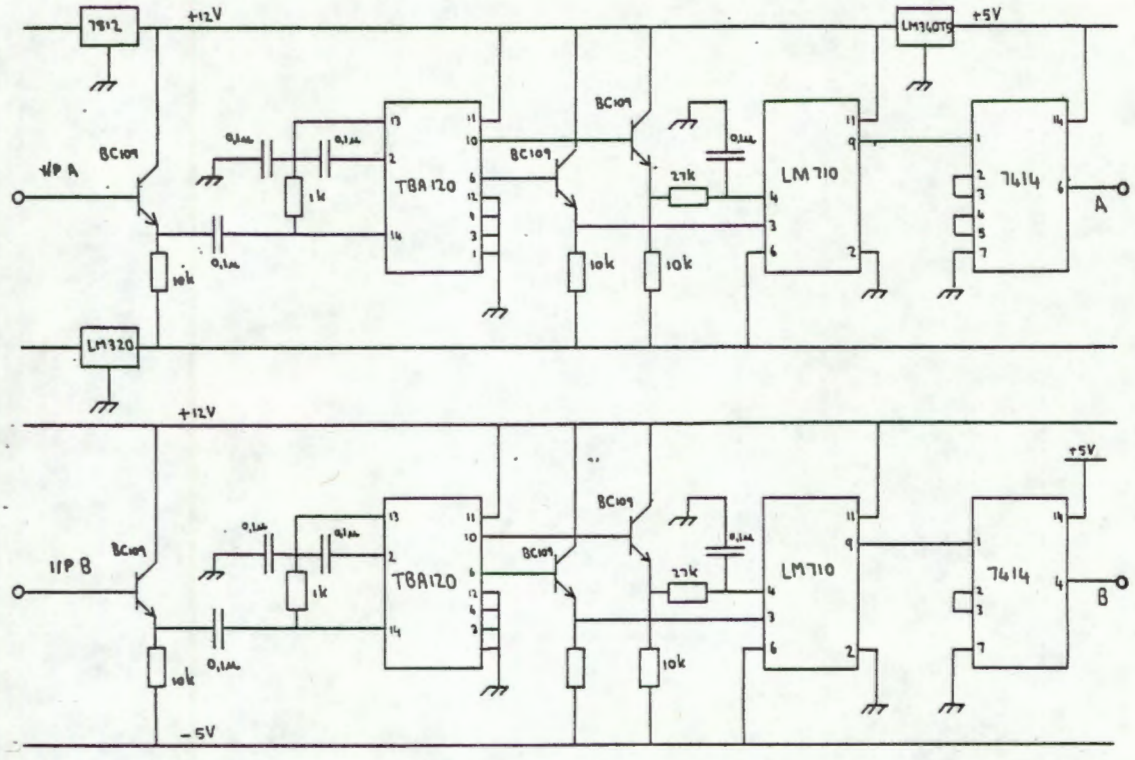

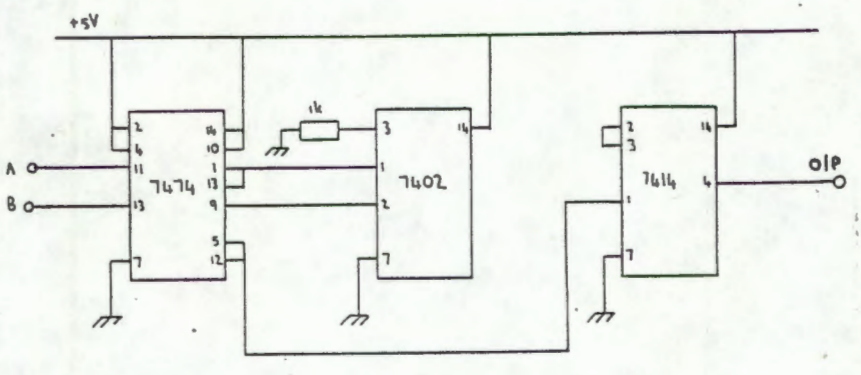

Fig. A.4 Phasemeter circuit diagrams.

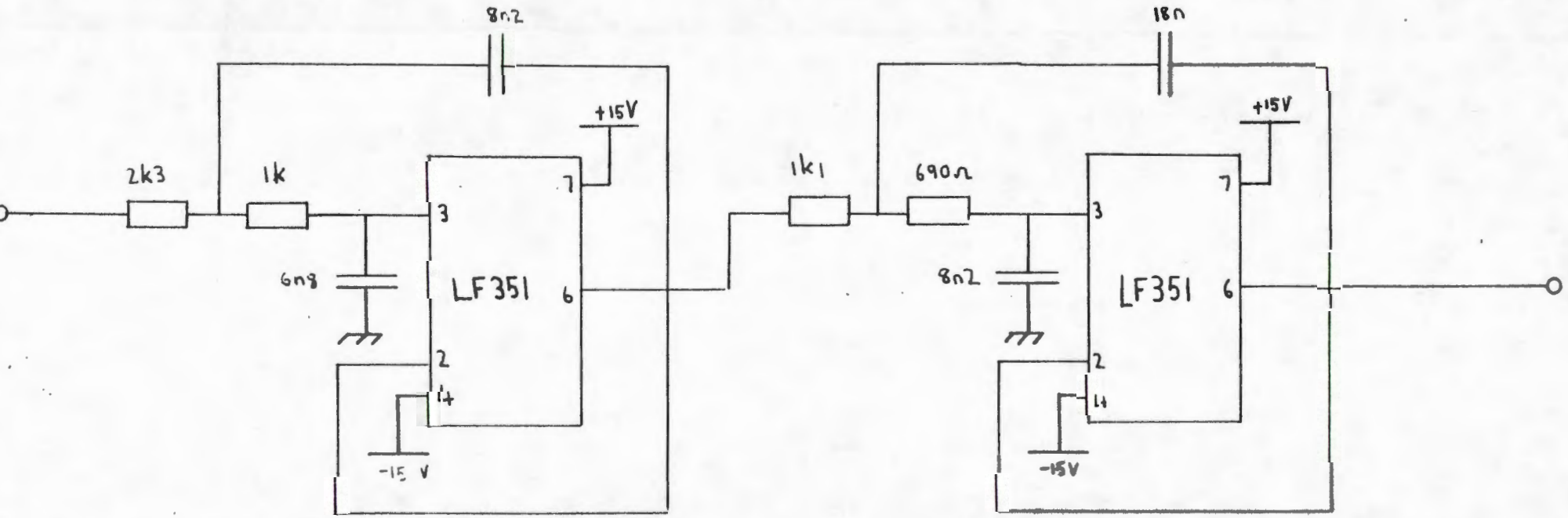

Fig. A.5 4^{th} order Butterworth low pass filter.
Cut-off frequency = 15 kHz.

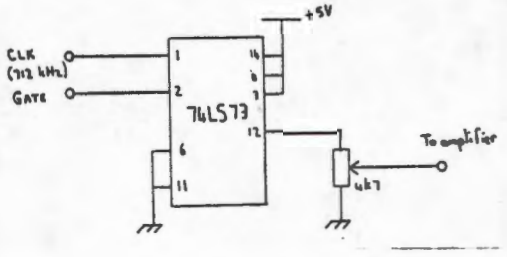

Fig. A.6 Transmitter gating circuit.

APPENDIX B

TRANSDUCER EQUIVALENT CIRCUIT AND CIRCLE DIAGRAMS

A Piezoelectric transducer operated close to resonance as a receiver may be represented by the following equivalent electrical circuit.

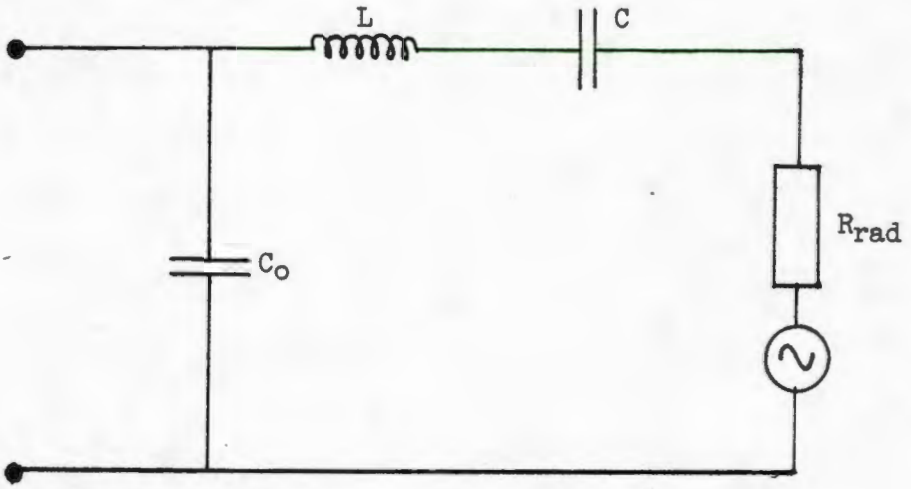

Fig. B.1 Transducer equivalent circuit.

The component values may be determined from the transducer 'circle' diagram. These are plots of susceptance against conductance for various frequencies. The 'circle' diagrams of the four transducers comprising the receivers are shown below. The resonant frequency and 3 dB points indicating the transducer bandwidths are indicated.

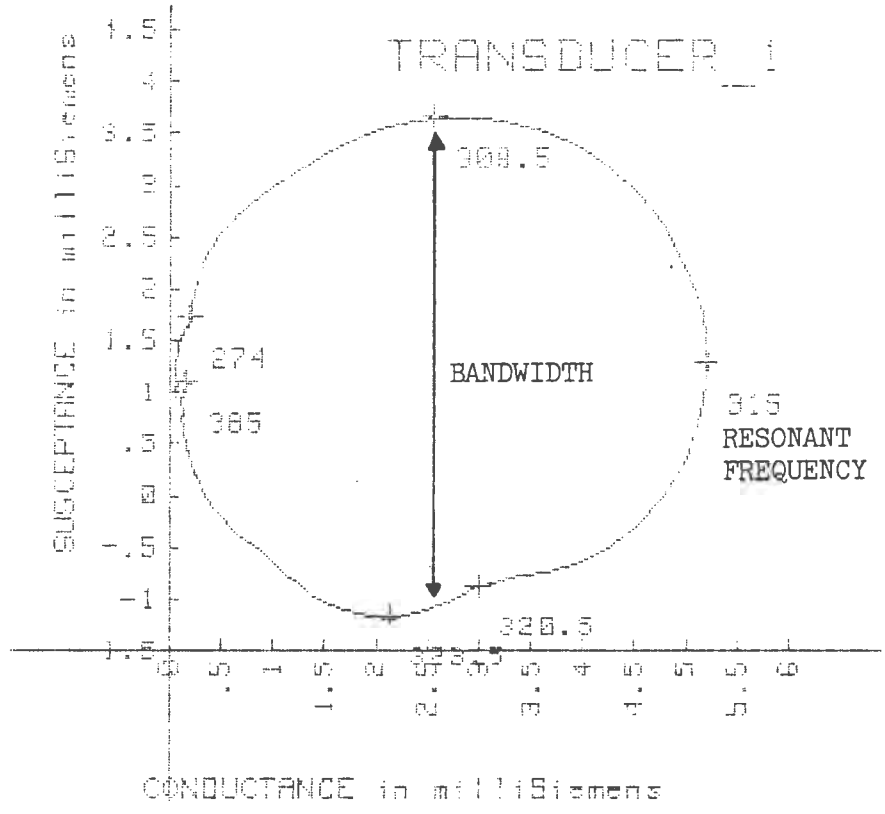

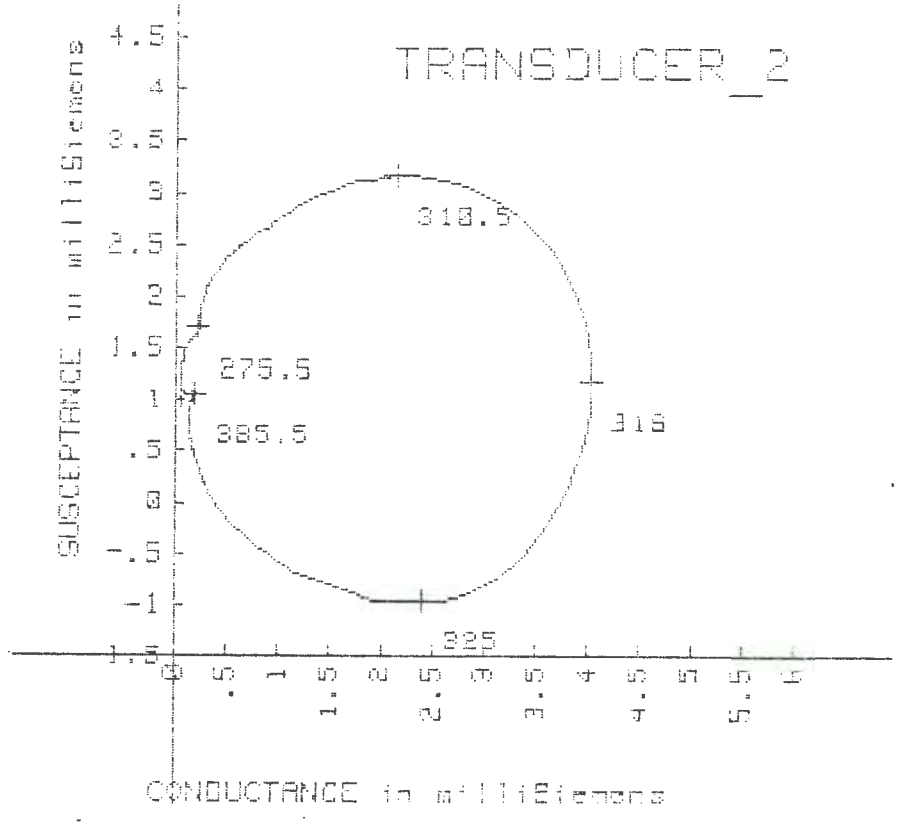

Fig. B.2 Receive transducer 'circle' diagrams.

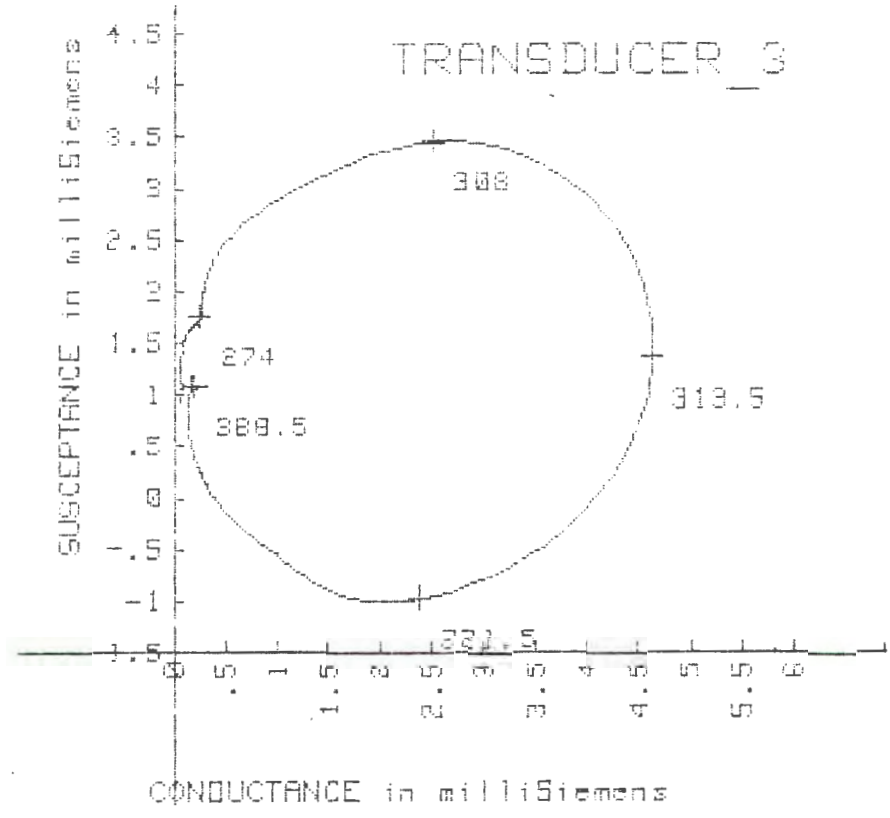

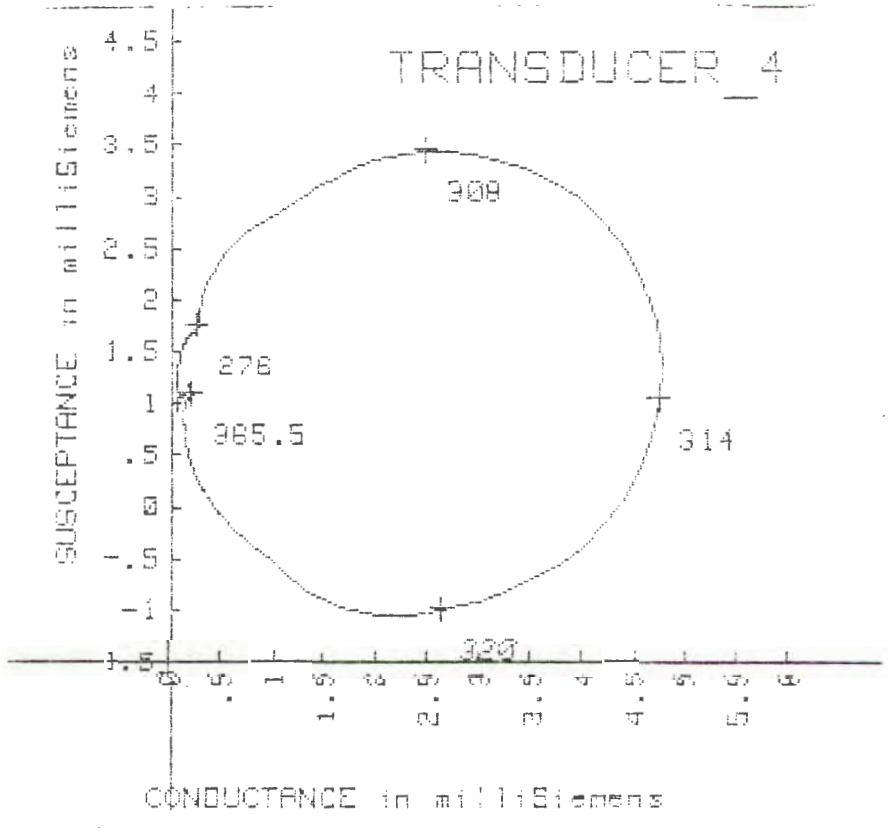

Fig. B.2 Receive transducer 'circle' diagrams.

As an example, the equivalent circuit parameters for transducer 1 are determined below.

The radiation resistance is the inverse of the conductance occurring at resonance : R_{rad}=190 Ω. The clamp capacitance is the susceptance occurring at resonance : C_o=0.7 nF. The remaining circuit values are calculated from the following relationships.

$$Q = \frac{f_o}{B} = \frac{315}{321-310}$$

$$= 28.6$$

$$Q = \frac{\omega_o L}{R}$$

$$\Rightarrow L = \frac{190 \times 28.6}{2\pi \times 315 \times 10^3}$$

$$= 2.7 \text{ mH}$$

As $\omega_o^2 = 1/LC$

$$C = 95 \text{ pF}$$

To increase the efficiency of the energy transfer between the transducer and preamplifier, the inductance L_t of the preamplifier input transformer is chosen to tune out the transducer clamp capacitance at resonance. At resonance

$$\omega_o L_t = 1/\omega_o C$$

The inductance required tocancel the clamp capacitance of transducer 1 is

$$L_t = \frac{1}{(2\pi \times 315000)^2 \times 0.7 \times 10^{-9}}$$

$$= 365 \text{ µH}$$

The remaining transducer equivalent circuits and matching are determined in a similar fashion.

APPENDIX C

COMPUTER PROGRAM AND ALGORITHMS

```
10 ! Program for storing sonar envelope and phase waveforms during
20 ! field testing.
30 !
40 DIM Q$[50]
50 INTEGER A
60 CLEAR 7
70 ON KEY# 1,"PARAM" GOSUB 170
80 ON KEY# 2,"REC" GOSUB 320
90 ON KEY# 3,"DSPLY" GOSUB 450
100 ON KEY# 4,"GNDREF" GOSUB 630
110 ON KEY# 5,"EXP" GOSUB 940
120 ON KEY# 8,"EXP" GOSUB 940
130 CLEAR @ KEY LABEL
140 GOTO 140
150 !
160 ! Subroutine for selecting data capture window.
170 !
180 DISP "All times in micro-secs"
190 DISP
200 DISP "Sample interval: ";
210 INPUT S1
220 DISP "Delay before capture: ";
230 INPUT T1
240 DISP "Duration of capture: ";
250 INPUT T2
260 X1=T1/S1
270 X2=T2/S1
280 BEEP
290 RETURN
300 !
310 ! Subroutine sets up data capture window on oscilloscope.
320 !
330 CONTROL 7,15 ; 1,10
340 OUTPUT 708 USING "K" ; "SPR"
350 OUTPUT 708 USING "K" ; "USP /'
360 OUTPUT 708 USING "K" ; "TIME5-03"
370 S$=VAL$ (2*X1)
380 E$=VAL$ (2*X1+2*X2+2)
390 Q$="BGN "&S$&"/END "&E$&"/CNT 1/DAT ?"
400 OUTPUT 708 USING "K" ; Q$
410 BEEP
420 RETURN
430 !
440 ! Subroutine for downloading and displaying waveforms from
450 ! oscilloscope.
460 !
470 CLEAR @ GCLEAR
480 SCALE 1,X2,0,255
490 XAXIS 0,100
500 YAXIS 1,50
```

```
510 FOR T=1 TO X2
520 ENTER 708 ; Y
530 MOVE T,Y
540 PLOT T,Y
550 ENTER 708 ; Y
560 MOVE T,Y
570 PLOT T,Y
580 NEXT T
590 BEEP
600 RETURN
610 !
620 ! Subroutine for determining the digital values corresponding
630 ! to the grounds  of the oscilloscope channels.
640 ! Enables digitized data to be referenced to ground.
650 !
660 CLEAR @ GCLEAR
670 DISP "Ground SCOPE inputs"
680 DISP "Press CONT"
690 BEEP
700 PAUSE
710 M=0
720 CONTROL 7,16 ; 1,10
730 OUTPUT 708 USING "K" ; "SPR"
740 OUTPUT 708 USING "K" ; "USP /"
750 OUTPUT 708 USING "K" ; "TIME-03"
760 OUTPUT 708 USING "K" ; "BGN 1/END 203/CNT 1/DAT ?"
770 WAIT 1000
780 A=0
790 C=0
800 FOR T=1 TO 100
810 ENTER 708 ; B
820 A=A+B
830 ENTER 708 ; B
840 C=C+B
850 NEXT T
860 F1=A/100
870 F2=C/100
880 DISP "CH1 Average=";F1
890 DISP "CH2 Average=";F2
900 BEEP
910 KEY LABEL
920 RETURN
930 !
940 ! Subroutine providing control of oscilloscope and stepper
950 ! motor during the mapping of the dam floor.
960 !
970 RESET 7
980 CLEAR
990 DISP "Number of swathes: ";
1000 INPUT N1
1010 DISP "Number of steps/swathe: ";
1020 INPUT N2
1030 DISP "No. PINGS/SWATHE: ";
1040 INPUT N3
1050 DISP "ENVELOPE data file: ";
1060 INPUT N$
1070 DISP "PHASE data file: ";
1080 INPUT P$
1090 PRINT ALL
1100 DISP "ENVELOPE data-file: ";N$
1110 DISP "PHASE data file: ";P$
```

```
1120 DISP "Swathes: ";N1
1130 DISP "Steps/swathe: ";N2
1140 DISP "PINGS/SWATHE: ";N3
1150 DISP "Sample int.: ";S1
1160 DISP "Delay: ";T1
1170 DISP "Duration: ";T2
1180 DISP "CH1 GND: ";F1
1190 DISP "CH2 GND: ";F2
1200 NORMAL
1210 RESET 7
1220 CREATE N$,N1*N3,X2*8
1230 CREATE P$,N1*N3,X2*8
1240 ASSIGN# 1 TO  N$
1250 ASSIGN# 2 TO  P$
1260 FOR B=1 TO N1
1270 FOR P=1 TO N3
1280 DISP "Swath#: ";B;" PING: ";P
1290 GOSUB 320
1300 FOR T=1 TO X2
1310 ENTER 708 ; A
1320 PRINT# 1 ; A
1330 ENTER 708 ; A
1340 PRINT# 2 ; A
1350 NEXT T
1360 NEXT P
1370 FOR T=1 TO N2
1380 CONTROL 3,2 ; 16
1390 WAIT 50
1400 CONTROL 3,2 ; 0
1410 NEXT T
1420 WAIT 2000
1430 NEXT B
1440 ASSIGN# 1 TO  *
1450 ASSIGN# 2 TO  *
1460 BEEP
1470 RETURN
1480 END
```

Data compression and smoothing algorithms.

The data compression and smoothing algorithms used during the production of the 3-dimensional picture are presented.

Data compression.

The phase and envelope waveforms were oversampled at the dam site. The volume of data to be processed was reduced by compressing the raw phase data. This was achieved by replacing groups of 5 successive phase values with their mean. If ϕ_1, $\phi_2, \phi_3, \ldots, \phi_{1000}$ are the raw phase data values and P_i is the i^{th} compressed phase value, then

$$P_i = (\phi_{5i-4}+\phi_{5i-3}+\phi_{5i-2}+\phi_{5i-1}+\phi_{5i})/5$$

Spatial averaging.

Spikes in the compressed phase data were smoothed by spatial averaging. Spatial averaging of two kinds was performed.

Spatial averaging within a ping was carried out by replacing each compressed phase value with a weighted average involving itself the 5 previous and 5 future compresed phase values. The current data point was accorded the highest weighting while the weightings of the surrounding points decrease linearly. If S_i is the i^{th} spatially averaged phase value then

$$S_i = (P_{i-5}+2p_{i-4}+3P_{i-3}+4P_{i-2}+5P_{i-1}+6P_i+5P_{i+1}+4P_{i+2}+3P_{i+3}+2P_{i+4}+P_{i+5})/36$$

Spatial averaging from ping to ping was performed by replacing each smoothed phase value with a weighted average involving itself and the corresponding data values from the 5 previous and 5 future pings. If S_i, is the i^{th} smoothed phase value occurring during the j^{th} ping and $Q_{i,j}$ is the corresponding ping averaged value, then

$$Q_{i,j} = (S_{i,j-5}+2S_{i,j-4}+3S_{i,j-3}+4S_{i,j-2}+5S_{i,j-1}+6S_{i,j}+5S_{i,j+1}+4S_{i,j+2}+3S_{i,j+3}+2S_{i,j+4}+S_{i,j+5})/36$$

It should be noted that the smoothing described above results in the loss of the first and last 5 data points from each ping as well as the data from the first and last 5 swaths.

APPENDIX D

DIRECTIVITY PLOTS

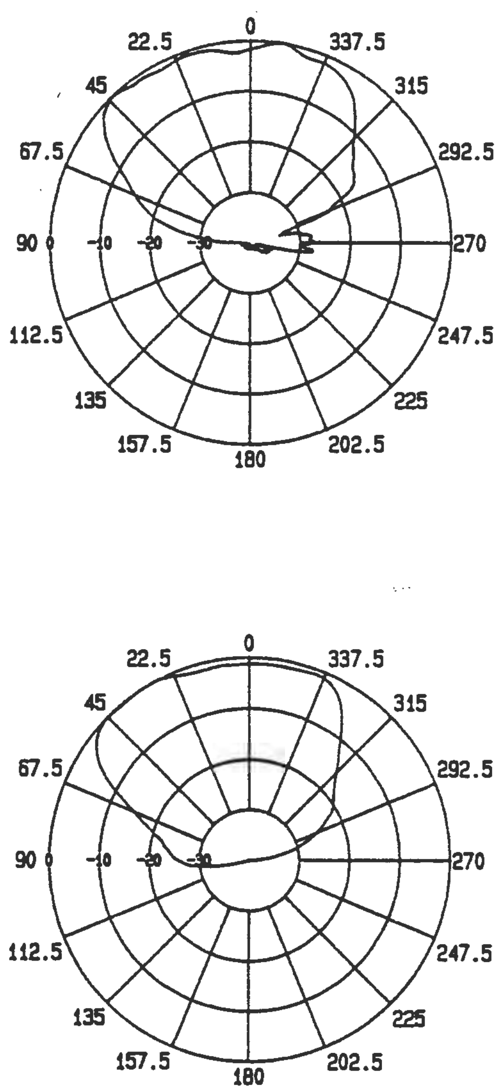

Transducer directivity plots for 3/4 wavelength Polycarbonate configuration.

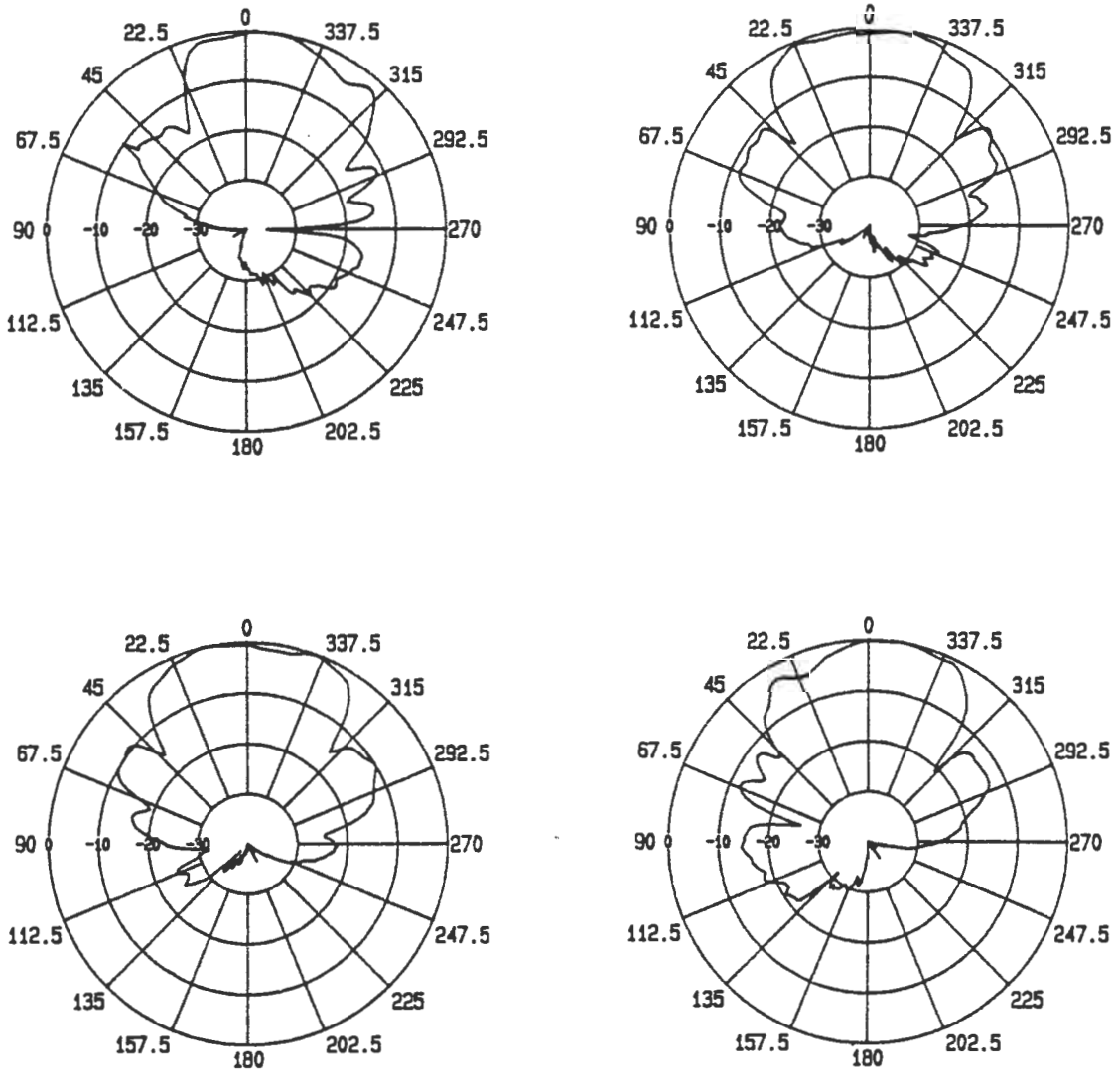

Transducer directivity plots for reference array.

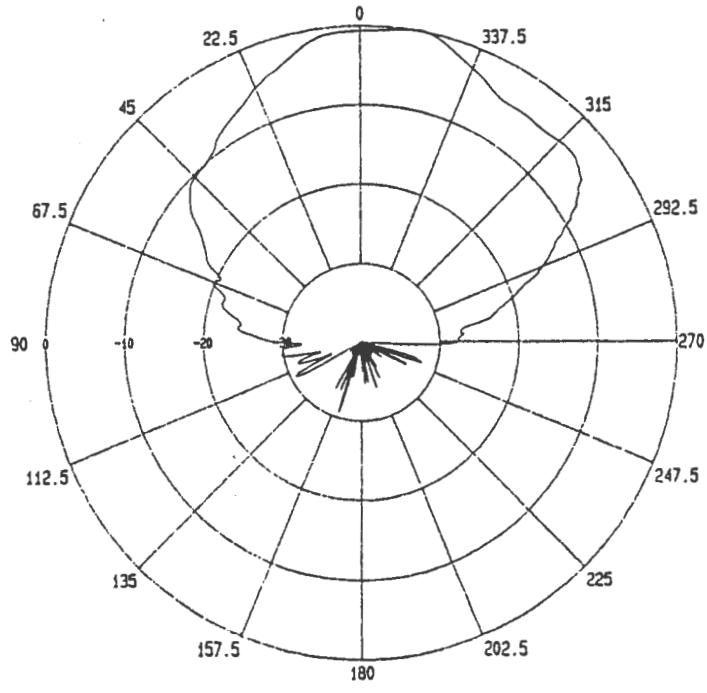

Vertical directivity plot for transmit array.

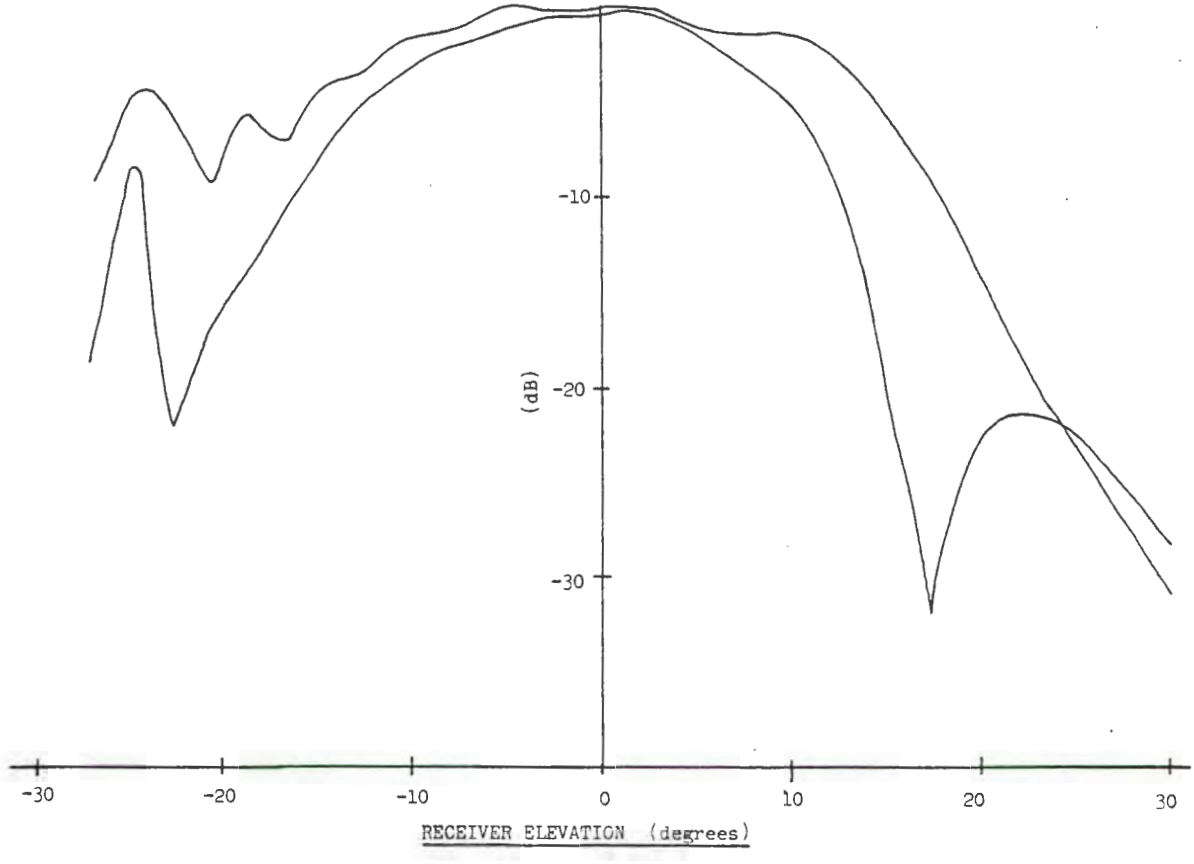

Vertical directivity plots for receiver/baffle combination used while mapping the dam floor.

APPENDIX E

SOFTWARE LOOK-UP TABLE

During the processing of the phase data captured at the dam site a software look-up table was used to convert the digitized phasemeter output to declination angle. Before generating the table, the receiver baffle combination was calibrated by recording the phasemeter output produced by the arrival of acoustic waves at angular increments within the unambiguous sector of the receivers.

The calibration was conducted in a water tank by mounting the receivers vertically from a stepper motor. The phasemeter output produced by a pulsed acoustic source was digitized and recorded at 0.38 degree intervals by stepping the motor.

A look-up table enabling the declination angle of the backscattered sound to be determined over an angular sector from 23.6 degrees to 53.3 degrees was created. As a finite motor step size was used during the calibration process, a number of phasemeter output states are skipped. Linear interpolation was used to ensure that each possible output state was assigned a declination angle. A graphical representation of the lookup table is shown in Fig. E.1.

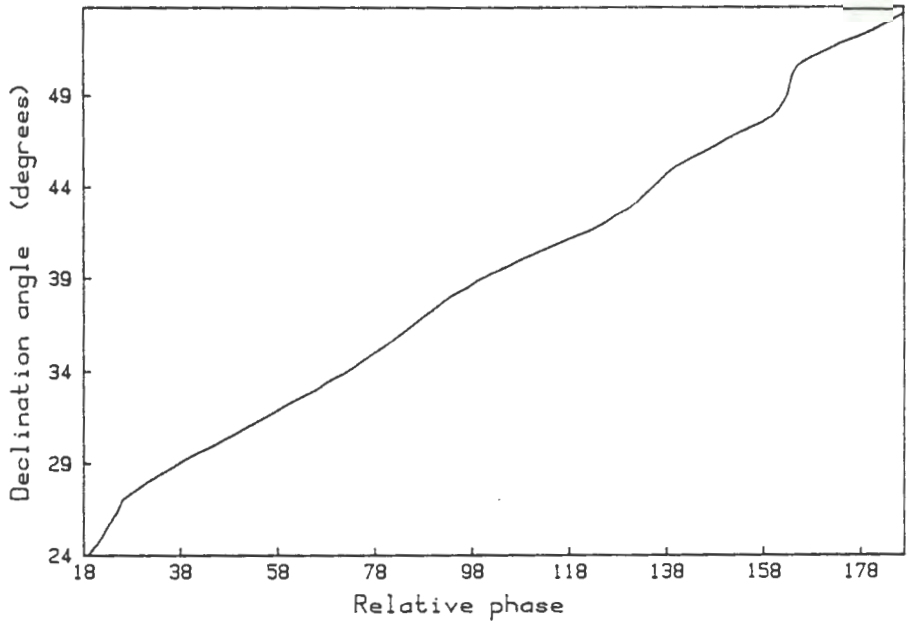

Fig. E.1 Graphical representation of software 'lookup' table.

APPENDIX F

MODEL PATH PARAMETERS

The relationships enabling the path parameters to be calculated for the forward and reverse path models are presented.

Forward path model

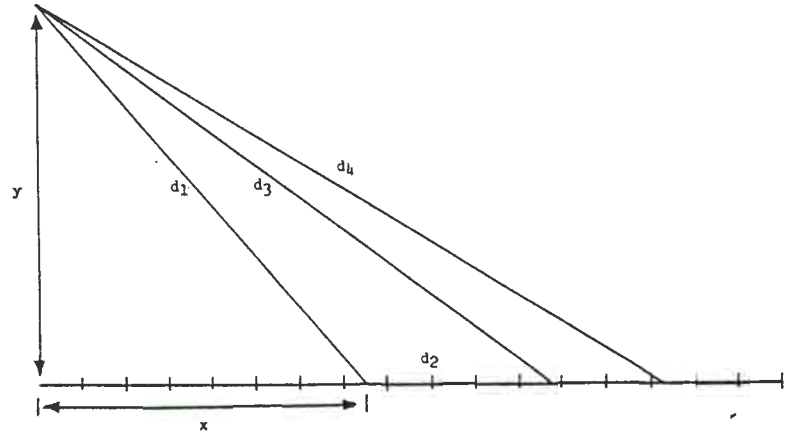

Fig. F.1 Forward path model geometry.

$$d_1 = \sqrt{x^2 + y^2}$$

$$d_2 = \frac{4d_4^2 - 4d_4\sqrt{x^2 + y^2}}{2x + 4d_4 - 2\sqrt{x^2 + y^2}}$$

$$d_3 = 2d_4 - d_1 - d_2$$

Reverse path model.

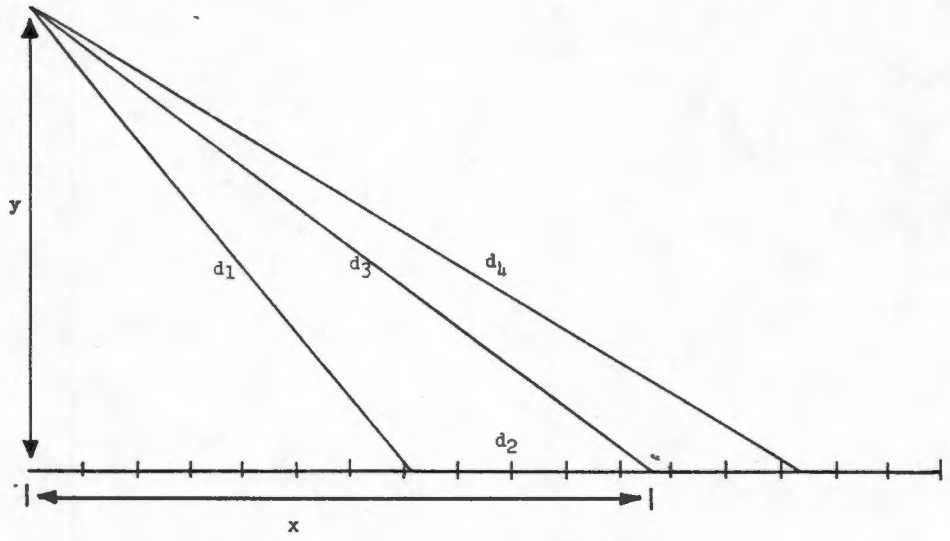

Fig. F.2 Reverse path model geometry.

$$d_3 = \sqrt{x^2 + y^2}$$

$$d_2 = \frac{4d_4d_3 - 4d_4^2}{2d_3 - 4d_4 + 2d_3\cos(\tan^{-1}(y/x))}$$

$$d_1 = 2d_4 - d_3 - d2$$

APPENDIX G

BISTATIC SCATTERING EXPERIMENT

The bistatic acoustic scattering of sound by a rough surface was examined by conducting a simple experiment in a water tank at the Central Acoustics Laboratory, University of Cape Town. Due to the small tank dimensions the experiment was conducted at a frequency of 4.5 MHz. This allowed the use of directive transmit and receive transducers, thereby eliminating echos caused by the spurious reflection of sound from the water surface and tank walls.

To determine the effect of increasing transmitter grazing angle on the amplitude of the sound scattered at small receiver grazing angles, an acoustic source producing 50 μs 4.5 MHz sinusoidal pulses was positioned to insonify a rough scattering surface at a grazing angle of approximately 2 degrees. The surface consists of a sand epoxy mixture over which a number of small irregular Polystyrene lumps are distributed. The scattering surface is shown in Fig. G.1.

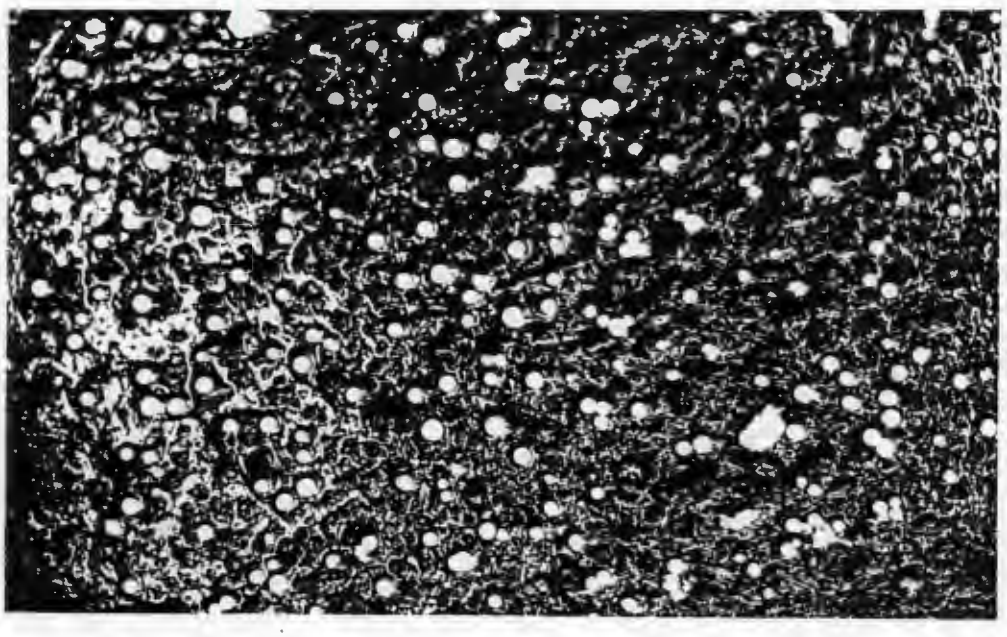

Fig. G.1 Scattering surface.

The scattering surface was clamped against a wall of the water tank. The amplitude of the sound backscattered from the surface was determined by placing a receiver close to the transmitter grazing angle and observing its amplified output on an oscilloscope. The transmitter grazing angle was increased and the resulting receiver output observed. The positions of the transmitter relative to the scattering surface is shown for the two measurements in Fig. G.2.

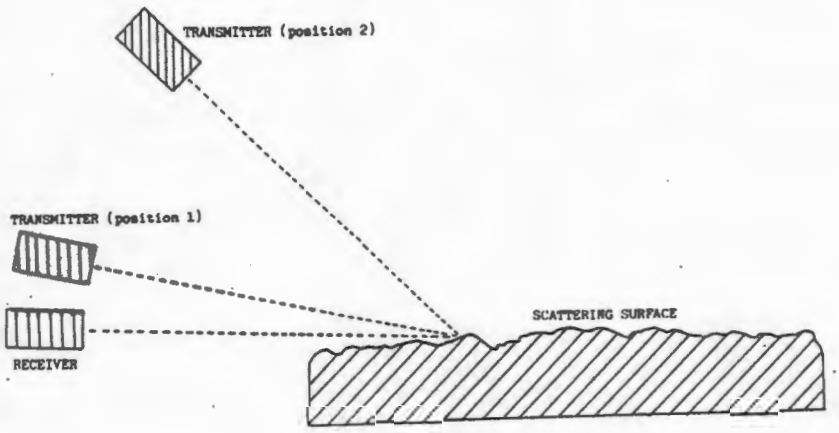

Fig. G.2 Transducer geometry.

Typical receiver outputs occurring at transmitter grazing angles of 2 degrees and 45 degrees are shown in Fig. G.3. The oscilloscope amplitude and timebase settings are 0.1 V/div and 50 μs/div respectively.

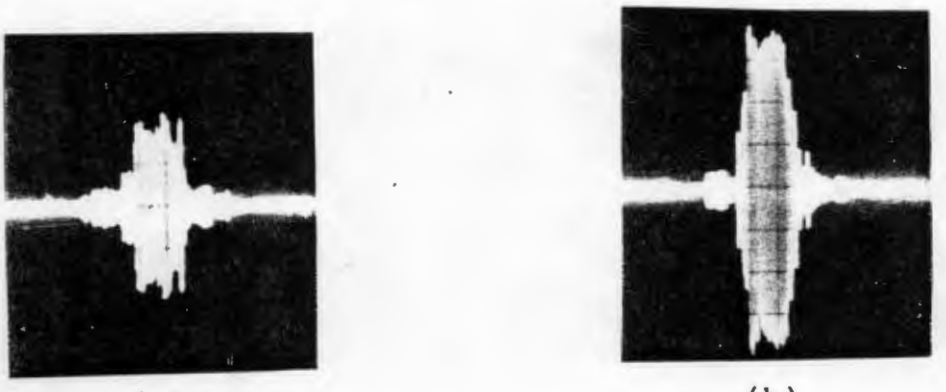

(a) (b)

Fig. G.3 Typical receiver outputs for a transmitter grazing angle of (a) 2 degrees (b) 45 degrees.

The increase in transmitter grazing angle results in a 6 dB increase in the amplitude of the sound scattered at the receiver grazing angle. While it should be noted that no attempt was made to deduce scattering strengths from the above measurements, they do indicate that the bistatic scattering strengths encountered at small receiver grazing angles are likely to be larger than the corresponding monostatic backscattering strengths.

22 JUN 1987